STRUCTURE AND PHYSICAL PROPERTIES OF HYDROGROSSULAR MINERAL SERIES

A THESIS IN

PHYSICS

Presented to the Faculty of the University of Missouri-Kansas City
in Partial requirements for the degree
MASTER OF SCIENCE

By

PUJA ADHIKARI

M.Sc, Tribhuban University, Kathmandu, Nepal, 2010

Kansas City, Missouri

2015

Structure and physical properties of Hydrogrossular mineral series

Puja Adhikari, Candidate for the Master of Science Degree

University of Missouri-Kansas City, 2015

ABSTRACT

The mineral hydrogrossular series ($Ca_3Al_2(SiO_4)_{3-x}(OH)_{4x}$; $0 \leq x \leq 3$) are important water bearing minerals found in the upper and lower part of the Earth's mantle. They are vital to the planet's hydrosphere under different hydrothermal conditions. The composition and structure of this mineral series are important in geoscience and share many commonalities with cement and clay materials. Other than the end members of the series x = 0 (grossular) and x = 3 (katoite) which have a cubic garnet structure, the structure of the series is totally unknown. We used large-scale *ab initio* modeling to investigate the structures and properties for hydrogrossular series for x = 0, 0.5, 1, 1.5, 2, 2.5, 3. Results indicate that for x > 0 and x < 3, the structures are tetragonal. This shows that there is structural change related to the lowering of overall symmetry associated with the composition of SiO_4 tetrahedra and AlO_6 octahedra. Total Bond order also explains the reason behind the change in the compressibility of the series. The electronic structure, mechanical and optical properties of the hydrogrossular series are calculated and the results for grossular and katoite are in good agreement with the available experimental data. The x–dependence of these physical properties for the series supports the notion of the aforementioned structural transition from cubic to tetragonal.

Key words: Hydrogrossular series, structural competition, electronic structure, mechanical properties, and optical properties.

APPROVAL PAGE

The faculty listed below, appointed by the Dean of the College of Arts and Sciences, have examined a thesis titled "Structure and Physical Properties of Hydrogrossular Mineral Series", presented by Puja Adhikari, candidate for the Master of Science degree, and certify that in their opinion it is worth of acceptance.

Supervisory Committee

Wai-Yim Ching, Ph.D., Committee Chair

Department of Physics and Astronomy

Da-Ming Zhu, Ph.D.

Department of Physics and Astronomy

Paul Rulis, Ph.D.

Department of Physics and Astronomy

CONTENTS

ILLUSTRATIONS

Figure Page

TABLES

Table Page

ACKNOWLEDGEMENTS

I would like to express my sincere gratitude to my advisor Dr. Wai-Yim Ching .I will be grateful to him forever for giving me an opportunity with encouragement, motivation, supervision, patience and support throughout my research.

I am thankful to Dr. Paul Rulis for always being there and helping me throughout the research with valuable suggestions. I would like to thank Dr. Da-Ming Zhu and Dr. James Murowchick for their valuable suggestions. My parents, Dr. Nav Raj Adhikari and Mrs Aruna Baba Bhattarai Adhikari are the source and pillars of motivation in my research and life. I appreciate all the support I got from my brother Apurba and sister Upama.

I am also thankful and appreciate all the help I got from Dr. Chamila Dharmawardhana, Mr. Jay Eifler and Mr. Lokendra Poudel and Electronic Structure Group. I also appreciate all the support I got from Computational Physics Group especially Dr. Naseer Dari and Mr. Ben Walker for their help and time. I would also like to thank Mr. Gyanendra Bhattarai and Mr. Shailesh Dhungana for their motivation, support and cooperation.

Finally, I would like to thank University of Missouri-Kansas City, Department of Physics and Astronomy for all the support.

DEDICATION

To my Dad Dr. Nav Raj Adhikari and my Mom Mrs. Aruna Baba Bhattarai Adhikari.

Nothing can compensate hard work.

Dr. Wai-Yim Ching

CHAPTER 1

INTRODUCTION

1.1 General Overview

There has been rapid development in the field of material science and condensed matter physics. One of the reason for this is increase in highly intensive computational technology. The empowered computational technology is possible due to highly intellect algorithm and valid theoretical models.

Experimentally research may be costly, dangerous, may take enormous amount of time and difficult to conduct. To solve the problem we may need to change the method. Theoretical research is initiative for the work which has not been done experimentally. Therefore, plays important role to start the research. Initially, they are based on hypothesis and the process trying to prove reveals the real science, which might be completely opposite to the hypothesis or same.

Basically computational physics works on the ideas given by both theoretical and experimental physics. The ideas that describes the physical scenario of the system is then implemented to the system which leads to simulation. Simulation, is the process of mimicking the real system. One of the simulation package is *ab initio*. The term *ab initio* means from the beginning.

In this thesis, we have used *ab initio* calculation for the mineral series known as hydrogrossular (HG) series ($Ca_3Al_2(SiO_4)_{3x}(OH)_{4x}$; $0 \leq x \leq 3$). Vienna ab initio simulation package (VASP) and Orthogonalized linear combinations of atomic orbitals (OLCAO) packages both based on density functional theory (DFT) are used for this calculation. VASP is

used for geometrical optimization and stress related calculations. OLCAO is used for electronic structure calculation.

1.2 Hydrogrossular

The hydrogrossular (HG) series, $Ca_3Al_2(SiO_4)_{3-x}(OH)_{4x}$, $0 \leq x \leq 3$ [1, 2] are important water bearing minerals found in Earth's upper and lower mantles as they can efficiently store a large amount of hydrogen [3, 4]. Its structure belongs to the garnet group, one of the nominal anhydrous minerals which are stable under a wide range of hydrothermal conditions [4]. The structure of HG series are considered to be cubic or pseudo cubic [2]. HG is also known broadly and less precisely as grossular ($x = 0$), hibschite ($0 \leq x \leq 1.5$) and katoite ($1.5 < x \leq 3$) [5] depending on its composition parameter x. So far, there has been only a modicum information on the structure and properties of the HG series except for the end members (grossular, $x = 0$ and katoite, $x=3$).

In HG series, Si^{4+} is progressively replaced by $4H^+$ as x increases which leads to the formation of $(OH)_4$ groups, a process known as hydrogarnet substitution (HGS) [4, 6]. Thus, grossular is completely anhydrous and katoite is completely hydrated. As (SiO_4) is replaced by (OH), there is increase in number of atom, cell size, and disorder. There has been studies only the end members of the series and very few on $x = 1.28, 1.5$ [7-10].

Since the structure of the end members of the HG series have a garnet structure with cubic symmetry (space group Ia3d (No. 230)), it has been widely speculated and tentatively assumed that the whole series will preserve this cubic symmetry. However, this is still an unresolved issue that has been hotly debated over a long time with no conclusive evidence.

Martin and Donnay [11] argued that garnet structure could not hold "water" since its molar volume increases by nearly 20% from $x = 0$ to $x = 3$ at zero pressure during HGS. Here,

the “water” referred to is the so-called crystalline “water”, or the hydroxyl (OH) group in geology. Later Aines and Rossman [3] suggested that hydrogarnet could hold “water” since it is more compressible than pure anhydrous silicates garnets. The observed bulk modulus of 168.4 ± 0.7 GPa for grossular [7] and 52 GPa for katoite [9] respectively validates this hypothesis. However, the lack of understanding on the precise structure and mechanical property in the rest of the series raises a serious question on the fundamental issue of the nature of hydrating process in HG series.

Although the Si-free mineral katoite (x = 3) has not been found in nature [12, 13], it has been synthesized [14, 15] and considerable amount of calculations have been done [16, 17]. Information on the structure and mechanical properties of katoite and other members of HG series can give insight about the water storage in earth’s mantle [17]. An in-depth knowledge of the precise structure of such a mineral series that is capable of bearing extraneous condition of high pressure in Earth’s mantle and its capacity for hydrogen storage will be extremely valuable. The hydration process can reveal important information about the metamorphic procedures occurring during crystal growth [18]**.** Moreover, the structure of a mineral could impact upon its elastic properties and the velocity of sound propagation. Geologists could use this information to identify the presence of this water-bearing mineral in Earth’s mantle and in determining their precise compositions [7] for geological surveys and maps on mineral location and composition. Furthermore, geoscientist can predict the possible change in the mantle in presence of HG.

Though there has been lot of studies for the HG for more than hundred years [2, 5]. There is still lot to know about the intermediate members. Experimentally, it has been a great challenge to study the HG series because of the difficulties associated with sample synthesis

and characterization under extreme conditions. *Ab initio* simulation appears to be well suited for such investigation. Some computational studies on for silicate garnets have been done in recent years [17, 19-23].Our main focus for this thesis is to understand the stable structures in the HG series due the hydrogarnet substitution. To the best of our knowledge, very little information on the structure or mechanical property for the entire HG series exist, except for the end members and a few reports for x = 1.28. Some experimental data on lattice constants and refractive index are available [8] for intermediate compositions, which can be used to compare and validate the proposed structural models HG series.

Since the end members of the HG series at x = 0 and x =3 have the same crystal structure and symmetry; furthermore, HG is a complete solid solution this gives additional hint for the unknown intermediate members. Therefore, with the help of end members and DFT intermediate members model can be predicted. The search for the structure of intermediate members is basically a combinatorial problem. An exhaustive search for all possible combinations of substitutions for an arbitrary x is a daunting task. Some plausible criteria based on sound chemical and physical intuition must be judiciously applied to narrow down the possibilities for more detailed study. We limit our investigation to composition x = 0, 0.5, 1, 1.5, 2, 2.5 and 3. Careful analysis of the structures and detailed calculation on their properties lead us to conclude that there is a symmetry lowering from cubic to tetragonal structure related to the composition of SiO_4 tetrahedra and AlO_6 octahedra in HG series that has not been identified before. The comparison of a variety of calculated properties which experimental data provide the means of further validating our proposed structures and hypothesis on structural transition.

It is important to know how the structure changes in the series. Furthermore, how the mechanical and electronic properties changes in this series. The information on these properties will provide sufficient information to identify these intermediate members in the earth's mantle.

The outlay of this thesis is as follows. In the chapter 2 and 3 we describe the computational methods used in modeling the structure and in properties calculation. This is followed by description of the steps employed in building the appropriate models for the HG series in chapter 4. The results on the electronic structure, interatomic bonding, mechanical and optical properties are presented and discussed in Chapter 5. We end with a brief conclusion and provide our vision for further studies on this important material and related systems in Chapter 6.

CHAPTER 2

THEORETICAL BACKGROUND

Study of any system begins with the knowledge of physical properties of atoms and molecules, which leads to the study of many body Schrödinger's equation, a complicated and expanded problem.

$$H\Psi\left(\boldsymbol{r_1}, \boldsymbol{r_2} \cdots \boldsymbol{r_N}\right) = E\Psi(\boldsymbol{r_1}, \boldsymbol{r_2}, \cdots \boldsymbol{r_N}) \tag{2.1}$$

$$\left[-\sum_{j}^{M}\frac{\hbar^2}{2M_j}\nabla_j^2 - \sum_{i}^{N}\frac{\hbar^2}{2m_i}\nabla_i^2 + \sum_{j}^{M}\sum_{p>j}^{M}\frac{Z_j Z_p}{\left|\boldsymbol{R_j} - \boldsymbol{R_p}\right|} - \sum_{i}^{N}\sum_{j}^{M}\frac{Z_j e^2}{\left|\boldsymbol{r_i} - \boldsymbol{R_j}\right|} + \sum_{i}^{N}\sum_{q>i}^{N}\frac{e^2}{\left|\boldsymbol{r_i} - \boldsymbol{r_q}\right|}\right]\Psi(\boldsymbol{r_1}, \boldsymbol{r_2}, \cdots \boldsymbol{r_N}) = E\Psi(\boldsymbol{r_1}, \boldsymbol{r_2}, \cdots \boldsymbol{r_N}) \tag{2.2}$$

Where, i, q refer to electrons and j, p refer to nuclei. m is the mass of electron and M_j, Z_j are the mass and the proton number of j^{th} nucleus. r_i, R_j are the position vectors of the electrons and nuclei respectively. ∇_j^2 and ∇_i^2 are the Laplacian operators with respect to i^{th} electron and j^{th}nucleus. In above equation (2.2). The first term is kinetic energy of nuclei; second term is kinetic energy of electron; third term is Coulomb repulsion between nuclei; fourth term is Coulomb attraction between nuclei and electron and the fifth term is Coulomb repulsion between electrons.

This equation basically takes account of the interaction of electrons and nuclei but is nearly impossible to solve. There are many approach which have tried to solve it. One of the approach is Born–Oppenheimer. Since mass of nuclei is heavier than that of electron Born–Oppenheimer approximation assumes nuclei to be stationary compared to electron. Therefore

using this approximation the kinetic energy of nuclei can be neglected and repulsion between nuclei can be considered constant. Therefore equation (2.2) can be written as

$$\left[-\sum_{i}^{N} \frac{\hbar^2}{2m_i} \nabla_i^2 - \sum_{i}^{N} \sum_{j}^{M} \frac{Z_j e^2}{|\boldsymbol{r_i} - \boldsymbol{R_j}|} + \sum_{i}^{N} \sum_{q>i}^{N} \frac{e^2}{|\boldsymbol{r_i} - \boldsymbol{r_q}|} \right] \psi(\boldsymbol{r_1}, \boldsymbol{r_2} \cdots \boldsymbol{r_N}) \tag{2.3}$$

$$= E\Psi(\boldsymbol{r_1}, \boldsymbol{r_2}, \cdots \boldsymbol{r_N})$$

This is still too complicated to solve. Another approach used is Thomas-Fermi model using density functional simplify the many body system. It use electron density $n(\boldsymbol{r})$ where, $\boldsymbol{r} = (\boldsymbol{x}, \boldsymbol{y}, \boldsymbol{z})$ instead of wave function. Total energy of the system, sum of kinetic energy and potential energy can be obtained using density as the functional.

$$E_{TF} = T + U_{e-Z} + U_{e-e} \tag{2.4}$$

$$E_{TF} = \frac{3h^2}{10m_e} \left(\frac{3}{8\pi}\right)^{\frac{2}{3}} \int [n(\boldsymbol{r})]^{\frac{5}{3}} d^3\boldsymbol{r} + \int n(\boldsymbol{r}) V_N(\boldsymbol{r}) d^3\boldsymbol{r} + \frac{1}{2} e^2 \int \frac{n(\boldsymbol{r}) n(\boldsymbol{r'})}{|\boldsymbol{r} - \boldsymbol{r'}|} d^3\boldsymbol{r} d^3\boldsymbol{r'} \tag{2.5}$$

Where the first term is kinetic energy; second and third term is electron–nuclear and electron–electron interaction respectively. The kinetic energy here is merely an approximate. Moreover, the Thomas–Fermi model does not include the exchange energy of atom, from Pauli exclusion principle. Later Dirac added exchange effects to the Thomas–Fermi model.

Hartree Fock (HF) method is another approach of simplifying many-electron problem. In equation (2.5), the single electron wave function depends only on spatial coordinates of electron. But to describe electrons in a complete form, spin should be also be accounted. Let spin function $\sigma(s)$ be either $\alpha(s)$ or $\beta(s)$ for electron spin up and spin down respectively and $\psi_i(x_i)$ be the product of electron spin functions with spatial orbital function $\phi(r_i)$.

$$\sigma(s) = \alpha(s) \; or \; \beta(s) \tag{2.6}$$

$$\psi_i(\boldsymbol{x_i}) = \phi_i(\boldsymbol{r_i}) \, \sigma(s) \tag{2.7}$$

Since Pauli exclusion principle requires the total wave function of many-electron system must be antisymmetric with respect to the interchange of the coordinates of any two electrons. We define new function satisfying the Pauli exclusion principle known as Slater determinant for N electron system.

$$\psi_{HF}(\boldsymbol{x_1}, \boldsymbol{x_2}, \cdots \boldsymbol{x_i}, \cdots \boldsymbol{x_N}) = \frac{1}{\sqrt{N!}} \begin{vmatrix} \psi_1(\boldsymbol{x_1}) & \psi_2(\boldsymbol{x_1}) & \psi_3(\boldsymbol{x_1}) & \cdots & \psi_N(\boldsymbol{x_1}) \\ \psi_1(\boldsymbol{x_2}) & \psi_2(\boldsymbol{x_2}) & \psi_3(\boldsymbol{x_2}) & \cdots & \psi_N(\boldsymbol{x_2}) \\ \psi_1(\boldsymbol{x_N}) & \psi_2(\boldsymbol{x_N}) & \psi_3(\boldsymbol{x_N}) & \cdots & \psi_N(\boldsymbol{x_N}) \end{vmatrix} \tag{2.8}$$

Where, constant $\sqrt{N!}$ normalizes $\psi(\boldsymbol{x_1}, \boldsymbol{x_2}, \cdots \boldsymbol{x_i}, \cdots \boldsymbol{x_N})$. The above equation satisfies the antisymmetric wave function since the exchange of two electrons, which can be explained as exchange of i^{th} and j^{th} column will change the sign of wave function of the system ψ. Furthermore, the determinant is totally antisymmetric in row too. If we have two electrons in one state the determinant will be zero which satisfies Pauli exclusion principle. We can simplify this by considering two electron system

$$\psi(x_1, x_2) = \frac{1}{\sqrt{2}} \begin{vmatrix} \psi_1(\boldsymbol{x_1}) & \psi_2(\boldsymbol{x_1}) \\ \psi_1(\boldsymbol{x_2}) & \psi_2(\boldsymbol{x_2}) \end{vmatrix} \tag{2.9}$$

If the two electrons are in same state at same time $\psi_1 = \psi_2$, then $\psi(\boldsymbol{x_1}, \boldsymbol{x_2}) = 0$.

Now we can calculate the energy expectation value by using following formula.

$$E_{HF} = < \psi_{HF} | \hat{H} | \psi_{HF} > \tag{2.10}$$

$$E_{HF} = \sum_{i=1}^{N} \boldsymbol{H_i} + \frac{1}{2} \sum_{i,j=1}^{N} (\boldsymbol{J_{ij}} - \boldsymbol{K_{ij}}) \tag{2.11}$$

Where,

$$\boldsymbol{H}_i = \int \psi_i^*(\boldsymbol{x}) \left[-\frac{1}{2} \nabla^2 + v(\boldsymbol{x}) \right] \psi_i(\boldsymbol{x}) d\boldsymbol{x} \tag{2.12}$$

$$\boldsymbol{J_{ij}} = \iint \psi_i(\boldsymbol{x_1}) \psi_i^*(\boldsymbol{x_1}) \frac{1}{\boldsymbol{r_{12}}} \psi_j^*(\boldsymbol{x_2}) \psi_j(\boldsymbol{x_2}) d\boldsymbol{x_1} d\boldsymbol{x_2} \tag{2.13}$$

$$\boldsymbol{K_{ij}} = \iint \psi_i^*(\boldsymbol{x_1})\psi_j(\boldsymbol{x_1})\frac{1}{\boldsymbol{r_{12}}}\psi_i(\boldsymbol{x_2})\psi_j^*(\boldsymbol{x_2})d\boldsymbol{x_1}d\boldsymbol{x_2} \tag{2.14}$$

Integral are real here. $\boldsymbol{H_i}$ consist of kinetic and electron–ion potential energy. $\boldsymbol{J_{ij}}$ are known as Coulomb integral and comes from the charge distribution of N electrons. $\boldsymbol{K_{ij}}$ are known as exchange integrals, which accounts the Pauli exchange principle and gives effective repulsion between electrons of parallel spin. In HF approximation, each electron is assumed to repel only the average distribution of the other electrons and not on their instantaneous position. The drawback of this theory is correlation in the motion between two electrons with antiparallel spin is neglected. Therefore, fails to account the instantaneous interaction of electrons known as correlation energy, which was later added to it and adds computational cost and complexity in the calculation known as post Hartee Fock.

Density functional theory (DFT) is another approach, which includes both exchange energy and correlation energy. DFT is used for condensed matter physics immensely because of its budget able computational cost and versatility. It allows one to replace N electrons wave function and associated Schrodinger equation with electron density $n(\boldsymbol{r})$ [24].

Basically DFT begins from Thomas and Fermi. In 1920s Thomas and Fermi used statistical approach to approximate the distribution of electrons in an atom. Thomas (1927) stated "Electrons are distributed uniformly in six dimensional phase space for the motion of an electron at the rate of two for each h^3 of volume," and that there is an effective potential field that "is itself determined by the nuclear charge and this distribution of electrons." [24]

DFT is based on Hohenberg-Kohn (HK) theorem. Basically, HK theorem presents ground state energy important and shows a way to calculate the density by minimization. The first theorem allows electron density $n(r)$ instead of electron number N and potential $V(r)$.

"The external potential $V_{ext}(r)$ is determined, within a trivial additive constant, by the electron density $n(r)$." In addition, $n(r)$ determines the ground state energy as well as number of electrons [24, 25]. The ground state energy can be written as

$$E_V[n(\boldsymbol{r})] = \int n(\boldsymbol{r})V_{ext}(\boldsymbol{r})dr + F_{HK}[n(\boldsymbol{r})] \tag{2.15}$$

Where,

$F_{HK}[n(\boldsymbol{r})]$ is a universal functional, sum of the kinetic energy functional $T[n(\boldsymbol{r})]$ and electron-electron interaction functional $V_{ee}[n(\boldsymbol{r})]$. It depends only on the type of interacting particles is independent of the external potential $V_{ext}(r)$.

$$F_{HK}[n(\boldsymbol{r})] = T\,[n(\boldsymbol{r})] + V_{ee}[n(\boldsymbol{r})] \tag{2.16}$$

Where,

$$V_{ee} = J[n(\boldsymbol{r})] + E_{ncl} \tag{2.17}$$

With, $J[n(\boldsymbol{r})] = \frac{1}{2}\iint \frac{n(\boldsymbol{r})n(\boldsymbol{r'})}{|\boldsymbol{r}-\boldsymbol{r'}|}d\boldsymbol{r}\,d\boldsymbol{r'}$ classical Coloumb part and E_{ncl} is a non-classical term is contribution to electron–electron interaction and is major part of "exchange–correlation energy".

The second Hohenberg-Kohn theorem provides energy for the variational principle. "For a trial density $n(\boldsymbol{r})$ such that $n(\boldsymbol{r}) \geq 0$ and $\int n(\boldsymbol{r})d\boldsymbol{r} = N$, $E_0 \leq E_V[n(\boldsymbol{r})]$ [24]. Therefore, this theorem minimizes its energy functional $E_V[n(\boldsymbol{r})]$ without changing the number of electron N and external potential.

$$E_0 = \int n_0(\boldsymbol{r})\,V_{ext}(\boldsymbol{r}) + F[n_0(\boldsymbol{r})] \tag{2.18}$$

The minimization of energy, as given by Lagrange's method is

$$\delta\left\{E_V[n(\boldsymbol{r})] - \mu\left[\int n(\boldsymbol{r})dr - N\right]\right\} = 0 \tag{2.19}$$

$$\mu = \frac{\delta E_V[n(\boldsymbol{r})]}{\delta n(\boldsymbol{r})} = V_{ext}(\boldsymbol{r}) + \frac{\delta F_{HK}[n(\boldsymbol{r})]}{\delta n(\boldsymbol{r})} \tag{2.20}$$

Ground state density determines the external potential which proves first HK theorem. If F_{HK} is known we can apply it to any system but it is difficult because explicit forms in E_{ncl}, non–classical term and $T[n(r)]$ are not known.

In 1965, Kohn and Sham used indirect approach to the kinetic energy functional $T[n(r)]$. In analogy with the HK universal function $F_{HK}[n(\boldsymbol{r})]$ they used non interacting system.

$$F[n(\boldsymbol{r})] = T_s[n(\boldsymbol{r})] + J[n(\boldsymbol{r})] + E_{XC}[n(\boldsymbol{r})] \tag{2.21}$$

Where,

$$E_{XC}[n(\boldsymbol{r})] \equiv T[n(\boldsymbol{r})] + V_{ee}[n(\boldsymbol{r})] - T_s[n(\boldsymbol{r})] - J[n(\boldsymbol{r})] \tag{2.22}$$

E_{XC} is exchange–correlation energy, it consists of the very small difference between $T[n(\boldsymbol{r})]$ and $T_s[n(\boldsymbol{r})]$ and E_{ncl} non–classical term.

Minimizing similar to (2.19) and (2.20)

$$\mu = \frac{\delta T[n(\boldsymbol{r})]}{\delta n(\boldsymbol{r})} + V_{eff} \tag{2.23}$$

Where, the Kohn Sham effective potential is

$$V_{eff} = V_{ext}(\boldsymbol{r}) + \frac{\delta J[n(\boldsymbol{r})]}{\delta n(\boldsymbol{r})} + \frac{\delta E_{XC}[n(\boldsymbol{r})]}{n(\boldsymbol{r})}$$

$$V_{eff} = V_{ext}(\boldsymbol{r}) + \frac{\int n(\boldsymbol{r}')}{|\boldsymbol{r} - \boldsymbol{r}'|} d\boldsymbol{r}' + V_{XC}(\boldsymbol{r}) \tag{2.24}$$

With the exchange–correlation potential,

$$V_{XC}(\boldsymbol{r}) = \frac{\delta E_{XC}[n(\boldsymbol{r})]}{n(\boldsymbol{r})} \tag{2.25}$$

Equation (2.23) is same as we obtain from conventional DFT, when we apply it to system of non–interacting electrons moving in external potential $V_{eff}(\boldsymbol{r})$. And by solving the N one electron equations for the given $V_{eff}(\boldsymbol{r})$ we can obtain $n(\boldsymbol{r})$ that satisfies equation (2.24) Now using Schrodinger's equation

$$-\frac{1}{2}\left[\nabla^2 + V_{eff}(\boldsymbol{r})\right]\psi_i(\boldsymbol{r}) = \varepsilon_i \psi_i(\boldsymbol{r}) \tag{2.26}$$

The value of $\psi_i(\boldsymbol{r})$ obtained from equation (2.26) is used to obtain the electron density as given by following equation

$$n(\boldsymbol{r}) = \sum_{i}^{N} |\psi_i|^2 \tag{2.27}$$

Initially electron density $n(\boldsymbol{r})$ is a guessed then, we calculate the effective potential and solve Kohn Sham equation, followed by calculation of electron density. If it is self-consistent then we calculate other quantities like energy, forces etc. If not self-consistent then again go back to the calculation of effective potential. The Kohn Sham approach, although exact, is difficult to use because the exchange-correlation functional E_{XC} is unknown.

One of the methods of approximating the exchange–correlation functional is local density approximation (LDA). According to this approximation, the exchange–correlation functional is calculated as

$$E_{XC}(n) = \int \varepsilon_{XC}[n(\boldsymbol{r})]\, n(\boldsymbol{r})\, d\boldsymbol{r} \tag{2.28}$$

Where, ε_{XC} is the exchange–correlation energy of an electron in a homogenous electron gas of density $n(\boldsymbol{r})$.

LDA has long been used in solid state physics. It is able to describe many ground state properties of many-electron system. Despite this, it has its limitations. LDA approximates energy of a system correctly when the density is uniform. In case the density varies, LDA needs to be improved so as to incorporate the variation.

While LDA considers uniform density at a point $\boldsymbol{r}$, most of the real systems are spatially non-uniform. Hence, the spatial variation of electron density has to be included to determine the exchange–correlation energy functional. Including the spatial variation of electron density, the exchange–correlation energy functional is expressed as,

$$E_{XC}^{G}\ GA[n(\boldsymbol{r})] = \int d\boldsymbol{r}\ f\big(n(\boldsymbol{r}), \nabla n(\boldsymbol{r})\big) \tag{2.29}$$

Where, the integrand is a function of local density $n(\boldsymbol{r})$ and gradient of $n(\boldsymbol{r})$. Equation (2.29) is called generalized gradient approximation (GGA).

CHAPTER 3

SIMULATION PACKAGES AND METHODS USED

We use two simulation packages Vienna *ab initio* simulation package (VASP) and orthogonalized linear combination of atomic orbital (OLCAO) both based on Density Functional Theory (DFT), one of the efficient method in solving many body problem in condensed matter physics. Though based on the same theory these packages are different because of difference in basis set.

3.1 Vienna *ab initio* Simulation Package (VASP)

Vienna ab initio simulation package (VASP) was initially developed in 1993 by Kress and coworkers [26, 27]. Basically used for the efficient relaxation and geometric optimization. It is used for electronic structure calculations and quantum mechanical molecular dynamics. It is capable of using different approach for Schrödinger's equation solution either density functional theory, using Kohn–Sham equation or Hartree–Fock approximation, using Roothaan equations. In addition, hybrid functional including both density functional theory and Hartree–Fock approximation, Green's functions methods and many–body perturbation theory are available.

VASP uses plane wave basis set. It fastens the Hamiltonian operations and transformation between reciprocal and real space wave functions using Fast Fourier Transform (FFT) technique. Furthermore, no Pulay terms. The interactions among electrons and ions is explained by ultra-soft Vanderbilt pseudo potentials (US-PP) [28, 29] or by the projector–augmented wave (PAW) [30, 31] in VASP.

The PAW method is considered to be better than US-PP. In PAW potential the core is considered to be frozen and computationally comparable to pseudo potentials. Furthermore,

Perdew, Burke and Ernzerhof (PBE) [32] developed a gradient correction for improvement of exchange correlation functional and is one of the best GGA in VASP. Sometimes, LDA is considered to be better in expense of time.

For efficient matrix diagonalization residual minimization with direct inversion of the iterative subspace (RMM-DIIS) and blocked Davidson are used. Individually, RMM-DIIS is faster whereas, blocked Davidson is stable and slow. If both are combined then blocked Davidson algorithm is used in the first iteration and then followed with RMM-DIIS. Therefore, is very efficient for large system and self-consistent calculation.

In the process of relaxation, VASP have capabilities to control the movement of ions to some extent. For example, if the structure is not near equilibrium, the quasi-Newton algorithm using forces and stress tensor to search the directions to equilibrium works fast but may take structure to inequilibrium whereas, conjugate-gradient approximation works slowly and allows the movement toward the direction of equilibrium. In addition, VASP can be used for the force and stress related calculations.

Both serial and parallel version is available in VASP. The parallel version is efficient as well as accurate and works with computer clusters and the supercomputers. Parallelization over bands or over plane wave coefficients or over both are available in VASP. The parallelization is over bands only will cause memory problem although works fast since each core will work on individual band whereas parallelization over wave coefficients only works very slow since all computer core will work on every band. Parallelization over the combination of both is the recommended.

VASP mainly consists of four input files INCAR, KPOINTS, POSCAR and POTCAR. The INCAR is the most important input which has parameters to control the calculation by

what we want from calculation and how. Basically it controls everything like electronic convergence criteria, relaxation of ions only, volume only or both, and many more. It has so many parameters that some of them are already set to default and we need to change only few as required for the calculation. KPOINTS file consists of number of k-points which works in mesh form. The k-point for any calculation is specified based on the size of the cell and mesh required for it. POSCAR is the input file consisting of the fractional coordinates of the atoms and lattice vectors. Most important part about the calculation is optimizing the system that we get from POSCAR. The POTCAR file consists of potentials for all atoms, elements in POSCAR.

In present thesis, with the highly efficient parallelization the structural optimization and calculation of elastic properties for hydrogrossular series $Ca_3Al_2(SiO_4)_{3-x}(OH)_{4x}$ were done on supercomputers at the National Energy Research Scientific Computing Center (NERSC).
The number of plane wave is determined by cutoff energy, 600 eV is used as a cutoff for relaxation as well as stress calculations in this calculation. PAW–PBE is used. The electronic convergence limit 10^{-5} eV and ionic convergence limit 10^{-3} eV were used. Since the modelling of the series were executed on our own method we used ISIF = 3 for both ion and volume relaxation, leading to well optimized structure. Gamma points were used as k-points.

3.2 Orthogonalized Linear Combination of Atomic Orbitals (OLCAO)

Orthogonalized Linear Combination of Atomic Orbitals (OLCAO) was developed at UMKC [33, 34]. OLCAO package based on local density approximation (LDA) of Density Functional Theory (DFT) is capable of electronic structure and spectroscopic calculation of crystalline [35, 36], non-crystalline [37, 38], biomolecule [39-41] and other complex structures accurately and efficiently. In UMKC, Electronic Structure group (ESG) are working with this

package and Computational Physics Group (CPG) are improvising it for even more accurate calculation.

OLCAO chose atomic orbitals to describe the atomic electronic configuration to solve Schrödinger's wave equation in many electron system. Therefore, linear combination of atomic orbitals (LCAO) were used for wave function of many electron system. Later LCAO method was improvised by orthogonalized plane wave (OPW), which was able to do band structure calculations and was developed by Conyers Herring [42].

In OLCAO method, solid state wave function ψ_{nk} in Bloch functions

$$\psi_{nk}(\boldsymbol{r}) = \sum_{i,\gamma} C_{i\gamma}^{n}(\boldsymbol{k}) b_{i\gamma}(\boldsymbol{k}, \boldsymbol{r}) \tag{3.1}$$

Where, γ is serial number of atoms, n is band index and $\boldsymbol{k}$ is wave vector. i is the orbital quantum number which includes principle quantum number n and angular quantum number (l, m).The Bloch sum $b_{i\gamma}(\boldsymbol{k}, \boldsymbol{r})$ is

$$b_{i\gamma}(k, r) = \left(\frac{1}{\sqrt{N}}\right) \sum_{v} e^{i(\boldsymbol{k}\cdot\boldsymbol{R_v})} u_i(\boldsymbol{r} - \boldsymbol{R_v} - \boldsymbol{t_\gamma}) \tag{3.2}$$

Where, $\boldsymbol{R_v}$ is reciprocal cell lattice, $\boldsymbol{t_\gamma}$ is vector pointing to the positon of γ^{th} atom in the cell and $u_i(\boldsymbol{r} - \boldsymbol{R_v} - \boldsymbol{t_\gamma})$ are the atomic orbitals and consists of radial and angular part

$$u_i(\boldsymbol{r}) = \left(\sum_{j=1}^{N} A_j r^{n-1} e^{-\alpha_j r^2}\right) \cdot Y_{lm}(\theta, \phi) \tag{3.3}$$

Where, i represents quantum number n, l and m. Radial part $\sum_{j=1}^{N} A_j r^{n-1} e^{-\alpha j r^2}$ limits till N i.e., is number of Gaussian type of orbitals (GTO) and $Y_{lm}(\theta, \phi)$ is the angular part.

The radial part shows the GTOs. The two GTOs can be transformed in new GTO and this simplifies the evaluation of orbital interaction integrals. α_j are decaying exponents, distributed in geometric series and range from α_{min} to α_{max} of N members and are selected based on experience. Their values differ for every element in periodic table. Range for each are α_{min} 0.1 to 0.15; α_{max} 10^6 to 10^9; and N from 16 to 30. Database for these parameters are provided in OLCAO. We can use same set of α_j for all atoms of the same element and for all the orbitals of different quantum number i.This reduces the computational cost. The u_i in equation (3.3) consist of core orbitals, the occupied valence orbitals, and a variable number of additional empty orbitals. There are three basis used in OLCAO, minimal basis (MB), full basis (FB), and extended basis (EB). If core and orbital in valence shell of atom, occupied or unoccupied it is called MB. If additional empty orbitals of the next unoccupied shell is added then it is called FB. Furthermore, if additional empty orbital of the next unoccupied shell is added then it is EB, it is used for spectral calculations.

Here we briefly explain the method part specifically for OLCAO. In OLCAO, we use one-electron Kohn–Sham equation

$$\left[-\nabla^2+V_{e-n}(\boldsymbol{r})+V_{e-e}(\boldsymbol{r})+V_{xc}[n(\boldsymbol{r})]\right]\psi_{nk}(\boldsymbol{r})=E_n(\boldsymbol{k})\psi_{nk}(\boldsymbol{r}) \tag{3.4}$$

As we know, in left hand side first term is kinetic energy, followed by electron–nuclear, electron–electron Coulomb, and exchange–correlation. The exchange–correlation potential depends on electron density $n(\boldsymbol{r})$, which is obtained from summation over occupied states.

$$n(\boldsymbol{r})=\sum_{occ}|\psi_{nk}(\boldsymbol{r})|^2 \tag{3.5}$$

The exchange-correlation energy$E_{xc}(\boldsymbol{r})$,

$$E_{xc}=(\boldsymbol{r})\int n(\boldsymbol{r})\varepsilon_{xc}[n(\boldsymbol{r})]d\boldsymbol{r} \tag{3.6}$$

Therefore, we get

$$V_{xc}(\boldsymbol{r}) = \frac{d(n\varepsilon_{xc}[n])}{dn} = -\frac{3}{2}\alpha\left[\frac{3}{\pi}n(\boldsymbol{r})\right]^{\frac{1}{3}} \tag{3.7}$$

Where α has been approximated to be $\frac{2}{3}$ by Kohn and Sham.

In OLCAO, crystal charge density $n_{cry}(\boldsymbol{r})$ and one-electron crystal potential $V_{cry}(\boldsymbol{r})$ are sum of atom-centered functions consisting of Gaussians.

$$n_{cry}(\boldsymbol{r}) = \sum_{A} n_A(r - t_A) \tag{3.8}$$

Where,

$$n_A(\boldsymbol{r}) = \sum_{j-1}^{N} B_j e^{-\beta_j r^2} \tag{3.9}$$

The electron–nuclear and electron–electron Coulomb interaction V_{Coul} and the exchange–correlation potential V_{xc} can be written as

$$V_{coul}(\boldsymbol{r}) = V_C(\boldsymbol{r} - \boldsymbol{t_A}) \tag{3.10}$$

$$V_{xc}(\boldsymbol{r}) = \sum_{A} V_x(\boldsymbol{r} - \boldsymbol{t_A}) \tag{3.11}$$

Where,

$$V_C(\boldsymbol{r}) = -\frac{Z_A}{r}e^{-\zeta r^2} - \sum_{j=1}^{N} D_j e^{-\beta_j r^2} \tag{3.12}$$

$$V_x(\boldsymbol{r}) = \sum_{j=1}^{N} F_j e^{-\beta_j r^2} \tag{3.13}$$

Where, $V_C(\boldsymbol{r})$'s first term is potential near nuclei and Z_A is the atomic number of the atom at that site. Crystal potential as sum of atom-centered potentials

$$V_{cry}(\boldsymbol{r}) = \sum_{A} V_A(\boldsymbol{r} - \boldsymbol{t_A}) \tag{3.14}$$

To increase the efficiency of OLCAO we use same set of exponential β_j in the Gaussian expansion from eqn (3.8) to (3.13). For each atoms β_j are predetermined but the coefficients B_j, D_j and F_j are updated in each cycle of self-consistent iterations. Here, β_j have range from $\beta_{\min}$ to β_{max} and have geometric distribution. The $\beta_{\min}$, β_{max} and number of term cast N depends on Z and system.

By Kohn–Sham equation (3.4) or equivalent secular equation below, we can obtain band structure.

$$\left|H_{i\gamma,j\delta}(\boldsymbol{k}) - S_{i\gamma,j\delta}(\boldsymbol{k})E(\boldsymbol{k})\right| = 0 \tag{3.15}$$

Where, $S_{i\gamma,j\delta}(\boldsymbol{k})$ and $H_{i\gamma,j\delta}(\boldsymbol{k})$ are overlap and Hamiltonian matrix respectively.

$$S_{i\gamma,j\delta}(\boldsymbol{k}) = \langle b_{i\gamma}(\boldsymbol{k},\boldsymbol{r})|b_{j\delta}(\boldsymbol{k},\boldsymbol{r})\rangle \tag{3.16}$$

$$H_{i\gamma,j\delta}(k) = \langle b_{i\gamma}(\boldsymbol{k},\boldsymbol{r})|H|b_{j\delta}(\boldsymbol{k},\boldsymbol{r})\rangle \tag{3.17}$$

In equation (3.15) the matrix elements between the Bloch sums can be divided into three parts (i) core–core, (ii) core–valence, valence–core and (iii) valence–valence. For simplicity using "valence" term to include all non-core orbitals. Assuming, matrix element between cores Bloch sums on different sites are zero and using orthogonality condition. Orthogonalized Bloch sum $b_{i\alpha}^{v'}(\boldsymbol{k},\boldsymbol{r})$

$$b_{i\alpha}^{v'}(\boldsymbol{k},\boldsymbol{r}) = b_{i\alpha}^{v}(\boldsymbol{k},\boldsymbol{r}) + \sum_{j,\gamma} C_{j\gamma}^{i\alpha} b_{j\gamma}^{c}(\boldsymbol{k},\boldsymbol{r}) \tag{3.18}$$

Where, v is denoted for valence and c for the core portion of Bloch sums.

$$C_{j\gamma}^{i\alpha} = \langle b_{j\gamma}^{c}(\boldsymbol{k},\boldsymbol{r})|b_{i\alpha}^{v}(\boldsymbol{k},\boldsymbol{r})\rangle \tag{3.19}$$

$$C_{j\gamma}^{i\alpha^*} = \langle b_{i\alpha}^{v}(\boldsymbol{k},\boldsymbol{r})|b_{j\beta}^{c}(\boldsymbol{k},\boldsymbol{r})\rangle \tag{3.20}$$

Using orthogonality condition

$$\langle b_{j\beta}^{c}(\boldsymbol{k},\boldsymbol{r})|\, b_{i\alpha}^{v'}(\boldsymbol{k},\boldsymbol{r})\rangle = \langle b_{i\alpha}^{v'}(\boldsymbol{k},\boldsymbol{r})\big| b_{j\beta}^{c}(\boldsymbol{k},\boldsymbol{r})\,\rangle = 0 \tag{3.21}$$

Where v' is used to denote the orthogonalized valence Bloch sums. After the orthogonalization, as there is no core–core overlap between the Bloch sums.

The orthogonalization of core orbitals to valence orbitals and liberty to choose any of three types of basis set above makes OLCAO package versatile. Bond order (BO) using Mulliken scheme [43, 44] calculation measures the relative strength of a bond between two atoms. Therefore, MB is used here. Similarly, band structure and density of states uses FB. For spectroscopic calculation EB is used since the accuracy increases after including one more unoccupied orbital to FB.

Band structure $E_n(\boldsymbol{k})$, one of the elemental calculation of electronic property can be calculated in OLCAO. The gap between the top of valence band (VB) and bottom of conduction band (CB) gives knowledge if the system is a metal, a semi–metal, a half–metal, a semiconductor or an insulator. Basically, it is a plot of energy eigen values as a function of k–points in reciprocal space. The density of states (DOS) $G(E)$ of the system by sampling $E_n(\boldsymbol{k})$ throughout Brillion Zone (BZ)

$$G(E) = \frac{\Omega}{(2\pi)^3}\sum_{n}\int d^3k\,\delta\big(E - E_n(\boldsymbol{k})\big) \tag{3.22}$$

Where, Ω is volume of the unit cell.

Furthermore, based on the quantum number n, l, and m quantum number the DOS can be expanded to partial density of states (PDOS). OLCAO package uses Mulliken's population analysis scheme [44] to calculate the fractional charge and bond order $\rho_{\alpha\beta}$. From Mulliken scheme, the fractional charge $\rho_{i\alpha}^{m}$ is

$$1 = \int |\psi_m(\boldsymbol{r})|^2 d\boldsymbol{r} = \sum_{i,\alpha} \rho_{i,\alpha}^m \tag{3.23}$$

$$\rho_{i,\alpha}^m = \sum_{j,\beta} C_{i\alpha}^{m^*} C_{j\beta}^m S_{i\alpha,j\beta} \tag{3.24}$$

Now the bond order using Mulliken's scheme $\rho_{\alpha\beta}$

$$\rho_{\alpha\beta} = \sum_{n.occ} \sum_{j,\beta} C_{i\alpha}^{*m} C_{j\beta}^m S_{i\alpha,j\beta} \tag{3.25}$$

Where, the $S_{i\alpha,j\beta}$ are the overlap integrals between the i^{th} orbital in the α^{th}atom and j^{th} orbital in the β^{th} atom and $C_{j\beta}^m$ are the eigenvector coefficients of the m^{th} band, j^{th} orbital in the β^{th} atom.

For optical properties, we use the extended basis (EB) which includes an additional shell of unoccupied orbitals than the FB. The interband optical properties are usually presented in the form of frequency-dependent complex dielectric function.

$$\varepsilon(\hbar\omega) = \varepsilon_1(\hbar\omega) + i\varepsilon_2(\hbar\omega) \tag{3.26}$$

For the imaginary part $\varepsilon_2(\hbar\omega)$, first optical conductivity $\sigma(\hbar\omega)$ is calculated using Kubo–Greenwood formula [45].

$$\sigma_1(\hbar\omega) = \frac{2\pi e\hbar^2}{3m^2\omega\Omega} \sum_{n,l} |\langle n|p|l\rangle|^2 f_l[1 - f_n]\delta(E_n - E_l - \hbar\omega) \tag{3.27}$$

Where, f_l is Fermi–Dirac function of the occupied band state l. The energy conservation between the transition process between the occupied state l and unoccupied state n with energy E_l and E_n is maintained by the δ function.

The imaginary part of the dielectric function $\varepsilon_2(\hbar\omega)$ can be obtained by following relation

$$\varepsilon_2(\hbar\omega) = 4\pi\left(\frac{\sigma_1(\omega)}{\omega}\right) \tag{3.28}$$

The real part using Kramers-Kronig relation

$$\varepsilon_1(\hbar\omega) = 1 + \frac{2}{\pi}\int_0^\infty \frac{s\varepsilon_2(\hbar\omega)}{s^2 - \omega^2}\,ds \tag{3.29}$$

After the frequency dependent dielectric functions are obtained we can obtain electron energy loss function [ELF] and optical constants. Refractive index $n(\omega)$ can be obtained by following relation

$$n(\omega) = \sqrt{\frac{\sqrt{(\varepsilon_1^2(\omega) + \varepsilon_2^2(\omega)} + \varepsilon_1(\omega)}{2}} \tag{3.30}$$

For static refractive index, $\omega \to 0 \quad \varepsilon_2^2(\omega) \to 0$ using (3.30) we get

$$n = \sqrt{\varepsilon_1(0)} \tag{3.31}$$

3.3 Elastic and Mechanical Properties Calculations

Elastic and mechanical properties of materials are crucial in understanding the physical properties of the material. Among them the most important parameter is elastic constant, from which interatomic interactions, mechanical stability, material strength and internal structure can be obtained. Upgraded computer technology and improved methodology has made it possible for the *ab initio* calculation of mechanical properties of the system more accurately [46].

For the calculation of elastic constant there are two approaches using for *ab initio* calculations. One of them, based on the analysis of total energy of a crystal as a function of its volume or pressure. The total energy $E(V, \varepsilon)$ of the crystal can be expressed as:

$$E(V,\varepsilon) = E(V_0) + V\sum_{i=1}^{6}\sigma_i\varepsilon_i + \frac{V}{2}\sum_{i,j=1}^{6} C_{ij}\varepsilon_i\varepsilon_j + \cdots \tag{3.32}$$

Where, ε_i are strain components, σ_i are stress components and C_{ij} are the elastic tensors. By fitting the total energies obtained under different strains to a parabola near the energy minimum elastic constants are derived [47].

The second approach is based on *ab initio* stress–strain relationship a Nielsen and Martin scheme [48]. This approach firstly optimize the volume and atomic position of the system. Applying small strain magnitude ε (this calculation, ± 0.5%) to each fully relaxed system. Then using the Hooks law,

$$\sigma_i = \sum_{j=1}^{6} C_{ij}\varepsilon_j \tag{3.33}$$

Here, stress component σ_i (i = 1 to 6) is linearly dependent to the applied strain ε_j(j = 1 to 6) under small deformation and C_{ij} are the elastic constants. Equation (3.33) a gives six set of linear equations with six components of stress and 21 elastic constants ($C_{ij} = C_{ji}$). Solving these equations are highly intensive computationally calculation.

For the calculation of bulk mechanical properties using the elastic tensor C_{ij}, and compliance tensor S_{ij} three approaches are used. They are (a) Voigt's approach, (b) Reuss approach (c) Voigt–Reuss–Hill approximation

In Voigt's approach [49] , bulk modulus K_{Voight} and shear modulus G_{Voight} is given for upper limit

$$K_{Voigt} = \frac{1}{9}(C_{11} + C_{22} + C_{33}) + \frac{2}{9}(C_{12} + C_{13} + C_{23}) \tag{3.34}$$

$$G_{Voight} = \frac{1}{15}(C_{11} + C_{22} + C_{33} - C_{12} - C_{13} - C_{23}) + \frac{1}{5}(C_{44} + C_{55} + C_{66}) \quad (3.35)$$

In Reuss approach [50] , bulk modulus K_{Reuss} and shear modulus G_{Reuss} is given for lower limit

$$K_{Reuss} = \frac{1}{(S_{11} + S_{22} + S_{33}) + 2(S_{12} + S_{13} + S_{23})} \quad (3.36)$$

$$G_{Reuss} = \frac{15}{4(S_{11} + S_{22} + S_{33}) - 4(S_{12} + S_{13} + S_{23}) + 3(S_{44} + S_{55} + S_{66})} \quad (3.37)$$

Hill later averaged both Voigt and Reuss approach and this is known as Voight–Reuss–Hill approximation (VRH) [51].

$$K = \frac{K_{Voight} + K_{Reuss}}{2} \quad (3.38)$$

$$G = \frac{G_{Voight} + G_{Reuss}}{2} \quad (3.39)$$

$$E = \frac{9KG}{3K + G} \quad (3.40)$$

$$\eta = \frac{3K - 2G}{2(3K + G)} \quad (3.41)$$

Where, E is Young's modulus and η is Poisson's ratio.

CHAPTER 4

STRUCTURAL MODELING OF THE HYDROGROSSULAR SERIES

4.1 Construction of Model

The crystal structures of grossular (x = 0) [52] and katoite (x = 3) [15] are well known. Both have cubic structure and same space group symmetry (**Ia3d**). Early studies assumed that the whole series will be based on the same crystal structure [8]. We use grossular as our initial template to generate models for the entire series.

Table 1: Experimental Structural Data of Grossular [52]

Space group Ia3d (230)			
a = 11.845, b = 11.845, c =11.845			
α =90, β = 90, γ = 90			
Fractional Coordinates			
Atom	**x**	**y**	**z**
Si	0.3750	0.0000	0.2500
Al	0.0000	0.0000	0.0000
Ca	0.1250	0.0000	0.2500
O	0.0381	0.0449	0.6514

In **Table 1** the formula for the series is Ca_3Al_2 $(SiO_4)_{3-x}$ $(OH)_{4x}$, x =0 The unit cell of grossular (also see **Fig1 (a))** consists of 24 (SiO_4) tetrahedra connected to 16 (AlO_4) octahedra via bridging oxygen and has 160 atoms in the unit cell with cubic lattice of space group Ia3d As the general formula for the solid solution suggests the rest of the series can be systematically obtained by replacing a Si atom by 4H atoms, a process known as the hydrogarnet subsititution [HGS] [4] .

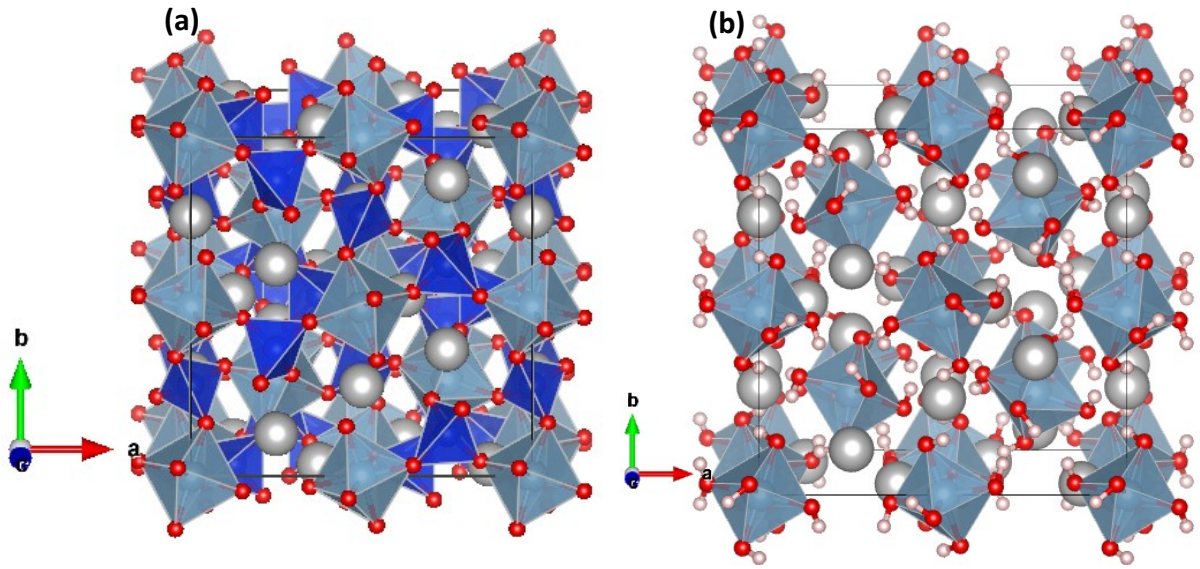

Figure1 Polyhedral diagram for relaxed Grossular (x=0) **(a)** and Katoite (x =3) **(b)** respectively. SiO_2 tetrahedra and AlO_6 octahedra are shown in a two different colors. Small red sphere, O; large grey sphere, Ca; small white sphere, H.

In the present studies we restrict ourselves to x = 0, 0.5, 1, 1.5, 2, 2.5, and 3.0. Generating structures by replacing Si by H atoms is basically a combinatorial process. For example, for x = 0.5 in $Ca_{24}Al_{16}Si_{20}O_{96}H_{16}$, 4 Si atoms are replaced by 16 H atoms and there are (24!)/(4!×20!) = 10,626 unique possible structures in the grossular unit cell. Possible combination for the other compositions we are listed in **Table 2**. The maximum number of combinations is 2,704,156 for x = 1.5. *Ab initio* simulations on all the possible combinations or even a portion of them will be impractical and prohibitively expensive. Thus, possible combinations must be significantly reduced by simple screening criteria based on basic chemical and structural intuitions.

Table 2: Composition, chemical formula for the unit cell, total possible combinations for constructing models, number of possibilities after criteria 1 and number of possibilities after criteria 2.

x	Formula	Total Combination	Criteria 1	Criteria 2	(# of Si)/Al
0	$Ca_{24}Al_{16}Si_{24}O_{96}$	1	1	1	6
0.5	$Ca_{24}Al_{16}Si_{20}O_{96}H_{16}$	10,626	10,626	24	5
1	$Ca_{24}Al_{16}Si_{16}O_{96}H_{32}$	735,471	733,023	255	4
1.5	$Ca_{24}Al_{16}Si_{12}O_{96}H_{48}$	2,704,156	2,413,732	640	3
2	$Ca_{24}Al_{16}Si_{8}O_{96}H_{64}$	735,471	247,095	255	2
2.5	$Ca_{24}Al_{16}Si_{4}O_{96}H_{80}$	10,626	24	24	1
3	$Ca_{24}Al_{16}O_{96}H_{96}$	1	1	1	0

To garner some insights, we start with comparing the structures of x = 0 and x = 3 as illustrated in **Fig. 1** showing the basic differences in the chemistry of the two crystals. The grossular (x=0) structure is very stable due to the strong silicate monomers gluing the relatively weaker aluminate octahedra. Silicate are well known to be the essential building block in the calcium silicate hydrate (CSH) minerals [53] which are chemically close to grossular as part of the more general calcium alumina silicate hydrate (CASH) family. In contrast, katoite (x = 3) is the completely hydrated phase of grossular and is structurally much less stable as indicated by the fact that it has not been found in Nature [12] . This provides the basis for the first stage of screening which we call **criterion 1**. We first tested a few models in which alumina octahedra were fully hydrated as illustrated in **Fig. 2(a)**. But accurate geometric optimization (see chapter 3) failed to converge indicating such structures are inherently unstable. Therefore, the presence of fully hydrated alumina unit shown in **Fig. 2(a)** should be avoided in modeling HG series. Hence, our criterion **1** in choosing the combinations is that every alumina octahedron has to be linked to at least one silicate tetrahedron. **Fig. 2(b)** illustrates a case in x=1.5 in which an alumina octahedron is associated with 3 Si tetrahedron. Next, a structure generating code was written which eliminates those combinations that have one or more fully hydrated aluminate units after substitution. The number of possible structures adhering to this scheme is tabulated in **Table 2**. For x = 1.5, it is reduced from 2,704,156 to 2,413,732, still way too large. Hence a more robust screening scheme, or **criterion 2** is devised to reduce it further. **Criterion** 2 is more intuitive. We make a plausible assumption that in HG series where a Si atom is progressively replaced by 4H atoms, the alumina octahedral unit gets partially hydrated at each x, the AlO_6 units are likely to be associated with the same number of SiO_4 units. Applying this rule, we found a pattern in which all alumina octahedra in the random

distribution can actually be connected to the same number of Si, i.e., the number of Si connected to each AlO_6 decreases from 6, 5, 4, 3, 2, 1, to 0 for the HG series from x = 0 to x = 3 as shown in **Table 2**. This is the **criterion 2**.

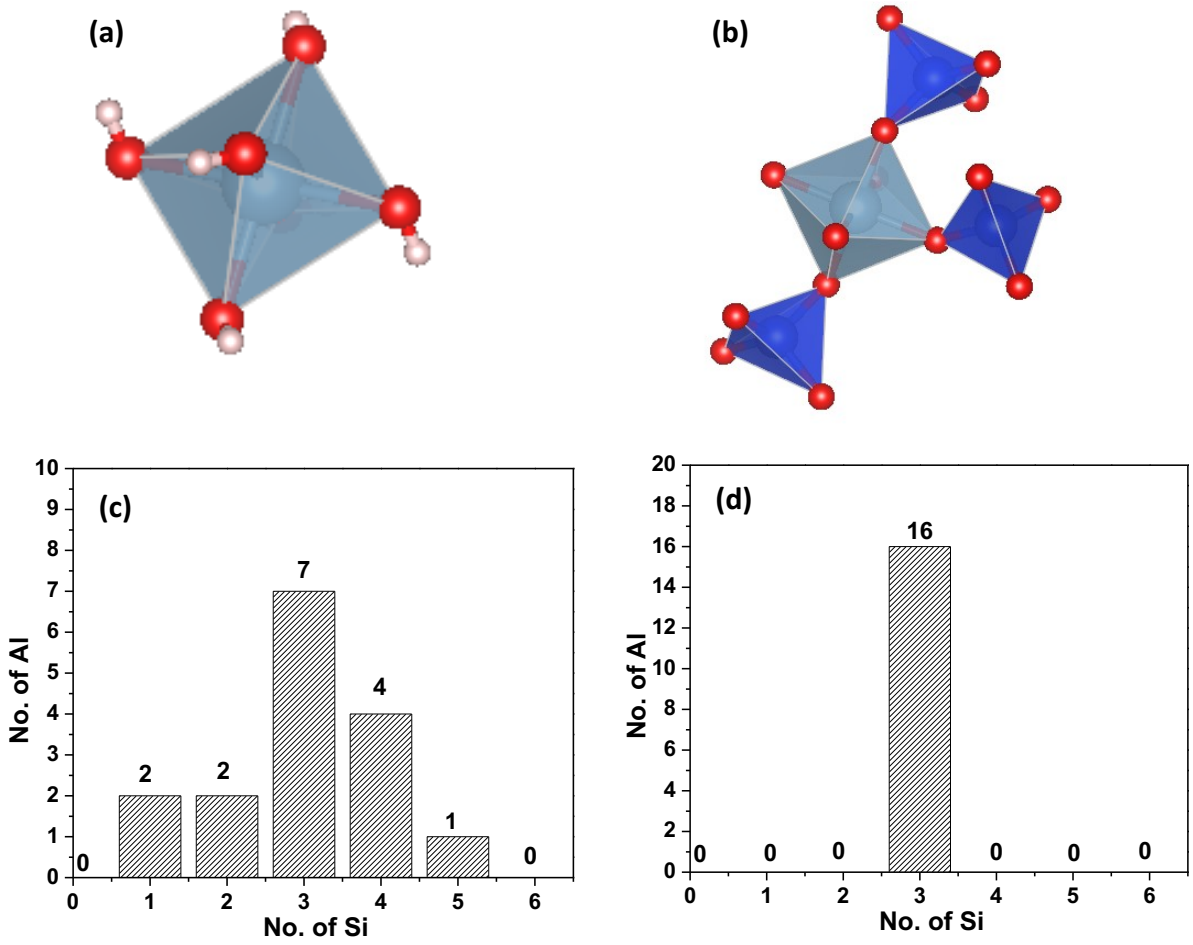

Figure 2 (**a**) Sketch of a fully hydrated alumina, (**b**) Al connected to three silicate tetrahedra according to **criterion 2** of uniformity for all alumina in x =1.5. Distribution of number of Si associated to Al octahedra for x = 1.5, (**c**) a randomly selected structure out of stable structures of criterion 1, (**d**) a special case with uniform connectivity following **criterion 2**.

The drastic reduction of number of possible structures in applying criterion 2 can be further illustrated for a specific case in x =1.5. The histogram distribution in **Fig. 2(c)** shows a randomly selected case after applying criterion 1. The 16 possible configurations for x=1.5 are: 2 AlO_6 linked with one SiO_4, 2 AlO_6 linked with 2 SiO_4, 7 AlO_6 linked with 3 SiO_4,….and so on. **Fig. 2(d)** shows distribution in which each AlO_6 in unit cell is linked to 3, and only 3 SiO_4 (**Fig. 2(b)**) according to criterion 2. Our selection of uniform distribution (Fig. 2(d)) over the random one (Fig. 2(c)) that can lead to a faster convergence in reaching a stable configuration is a reasonable choice since there is no evidence in literature that suggests any preferential substitution of silicates in HG series. Indeed our extensive tests involving geometric optimization, computational efficiency, and rate of convergence all indicate that the structures selected by applying the uniform condition are much more stable than the randomly substituted structures. We are thus convinced that this is the right strategy for obtaining the stable structures in the HG series for a given x**.**

4.2 Structural Analysis

At this point the filtering process based purely on the connectivity and distribution of silica on the basis of chemical and structural reasoning is almost exhausted. A further reduction was achieved via accurate *ab initio* calculations on selected samples. For example, for x = 0.5 and x = 2.5, the number of possible structures (**Table 1**) are 24 each. We are able to relax all 24 possible structures using *Vienna Ab initio Simulation Package* (VASP) (see chapter 3 for details). Results show that all 24 structures are tetragonal. For x = 1.0, 1.5 and 2.0, the possible number of structures are 255, 640 and 255 respectively. These are much reasonable numbers, but still exhaustive for *ab initio* calculations. We randomly chose 15 configurations for x = 1, 2 and 20 configuration for x = 1.5 and ranking them in terms of the calculated total energy.

The one with the lowest total energy is then designated as the representative model for that x. The lattice parameters for the final structure derived after the stringent criteria explained above are listed in **Table 3.** They are cubic for x = 0, 3.0 and tetragonal for x = 0.5, 1.0, 1.5, 2.0, 2.5. Apparently, there is structural transition in the series away from the end members in lowering the symmetry.

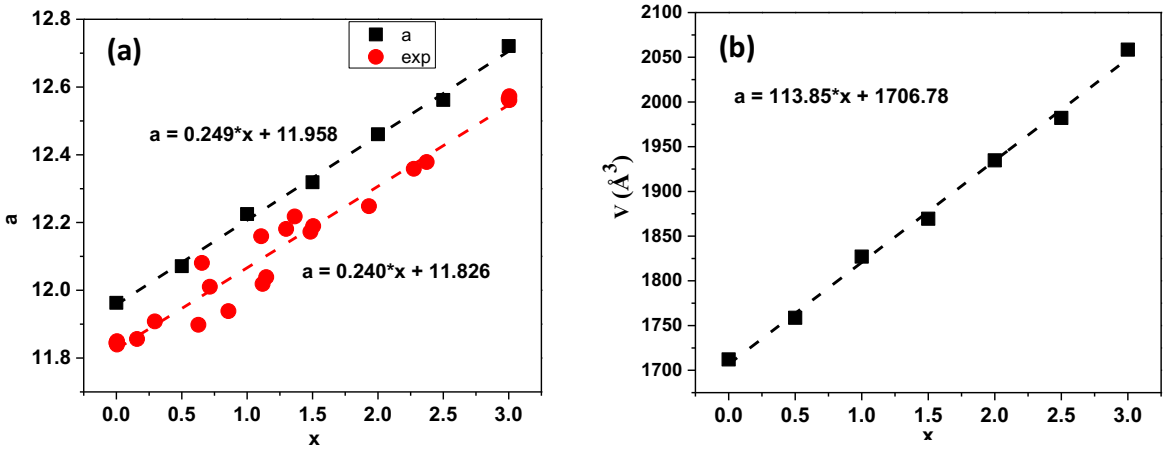

Figure 3 (a) Variation in lattice constant a as a function of composition (x)**.** Red solid circle shows experimental data [8]. Black solid square is the average of the lattice constants from our simulation. **(b)** Cell volume of the HG series as a function of composition (x)**.** The dashed lines are linear fit.

In **Fig. 3(a)**, we display the average of the lattice constants as a function of x and the experimental data [8, 54]. Also shown are the calculated volumes of the unit cell as a function of x. Of the 7 data points available (**fig. 3(b)**), there is a linear relationship which can be fitted to the equation: a = 0.249*x + 11.958 (for average lattice constant). A similar fit for the

experimental values give a = 0.240*x + 11.826. The almost identical slopes of fitting in the lattice constant is very gratifying sowing the validity of the simulated structure for HG series. The slight over estimation of the simulated value in comparison with the measure value is due to the use of GGA potential in the VASP relaxation which is a well-known drawback in the calculations based on density functional theory. (see the next section). A practical way for the analyses the model rigorously is to calculate the radial pair distribution function (RPDF).

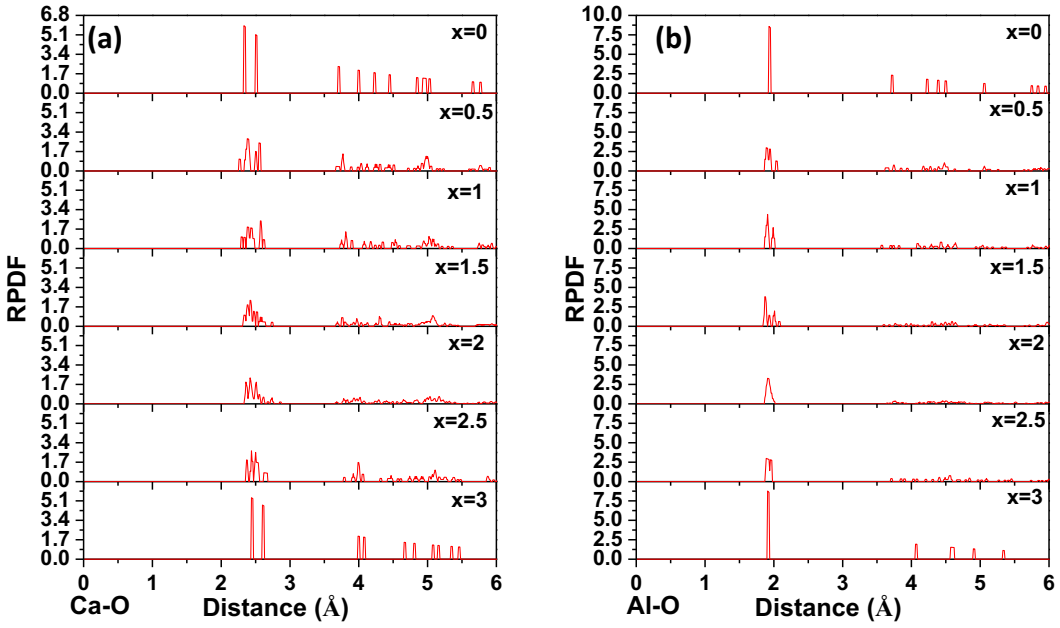

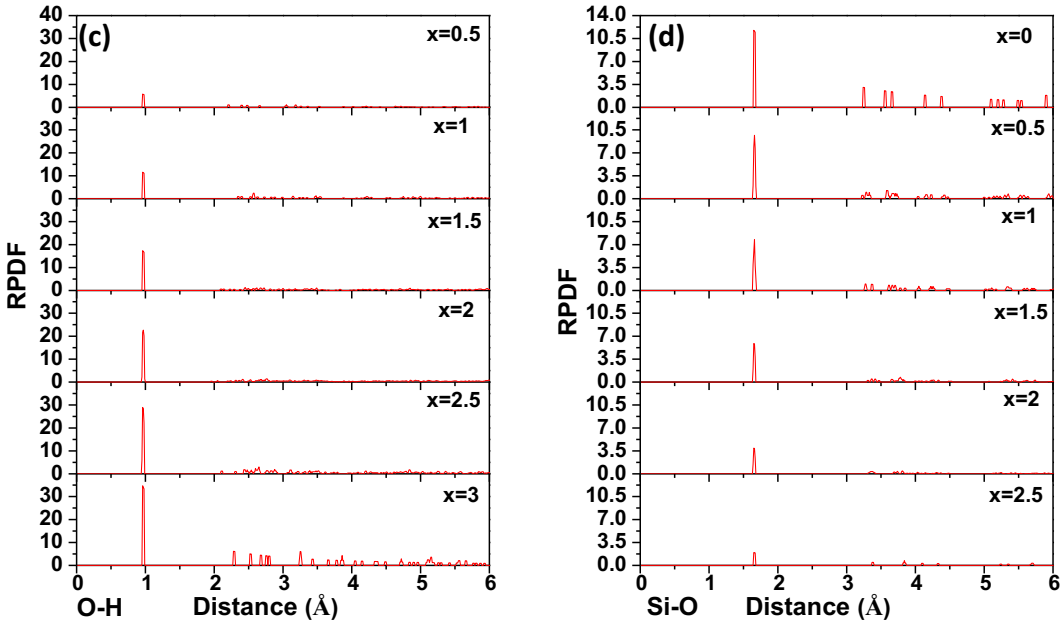

Figure 4 Radial pair distribution function of **(a)** Ca–O, **(b)** Al–O, **(c)** O–H and **(d)** Si–O of the hydrogrossular (HG) series

Fig 4 shows the calculated RPDF plots up to a radial distance of 6 Å between most important pairs of the hydrogrossular series. The peaks below 2 Å corresponds to nearest neighbor pairs in the series. **(a)** Ca–O has first two distinct peaks at around 2.33 Å, 2.50Å for x = 0 and 2.44Å, 2.60Å for x = 3. For the intermediate series they have the slightly broaden peaks but they fall within 2.27 Å to 2.76 Å. **(b)** Al–O also has first sharp peaks for x = 0 and 3 at around 1.93 Å and 1.91 Å respectively. Intermediate series have slightly broaden peaks from 1.85 Å to 2.09 Å. **(c)** O–H have a sharp peak for the series from x = 0.5 to 3 (no Hydrogen atoms in x = 0) at 0.96 Å. The peak increases from x = 0.5 to 3 because number of Hydrogen atoms increases (d) Si–O, also have a sharp peak for the series from x =0 to 2.5 (no Silicon

atoms in x = 3) within 1.65 Å to 1.66 Å. The peak decreases along the series from x = 0 to 2.5 because the number of Silicon atoms decreases

The key element Si and H which changes throughout the series have very sharp line authenticating the chosen models; furthermore, the SiO_4 tetrahedral is distributed uniformly throughout the series. From RPDF, we can say that there is no unusual bonding among the pairs since all of the pair bonds discussed above falls under the average bond length respectively. In addition, the end members x = 0 and 3 are crystalline whereas the intermediate members are not.

CHAPTER 5

ELECTRONIC AND MECHANICAL PROPERTIES OF HYDROGROSSULAR

In this section, we present detailed physical properties of the HG series using the *ab initio* OLCAO method [34] based on the fully relaxed structures of the HG series described in Chapter 3. The OLCAO method is particularly efficient for the electronic structure and interatomic bonding investigations for materials with complex structures and compositions as demonstrated in many recent publications [40, 55, 56], This section is divided into two subsections (i) electronic structure covering density of states with band structure, interatomic bonding, and optical properties (ii) mechanical properties including elastic stiffness and bulk mechanical properties respectively. These results provide a complete picture of the continuous change in properties as a function of HGS. The calculated results are found to be in good agreement with available data for the end members grossular (x = 0) and katoite (x = 3).

5.1 Electronic Structure of Hydrogrossular Series

5.1.1 Density of States and Band Structure

We first show the calculate band structure of grossular and katoite in the cubic structure containing 2 formula units since the primitive cell for garnet is b.c.c. **Fig. 5** shows both crystals have direct band gap (Eg) at Γ (4.90 eV for grossular and 3.91 eV for katoite). The top of the valence band (VB) is very flat as expected while the bottom of the conduction band (CB) shows some curvature at Γ. They are quite similar to the bands structure of yttrium aluminum garnet ($Y_3Al_5O_{12}$ or YAG) published early in 1999 [56] and used the BCC primitive cell. The calculated total density of states (TDOS) in the energy range from -20 eV to 20 eV for stable HG series phases are presented in **Fig. 6**. The zero of the energy is set at the top of the VB. The entire series consists of wide gap insulators. At a first glance, the features in the TDOS in

both the occupied VB and unoccupied CB are very similar. However, a closer inspection of peak structures show subtle differences as a

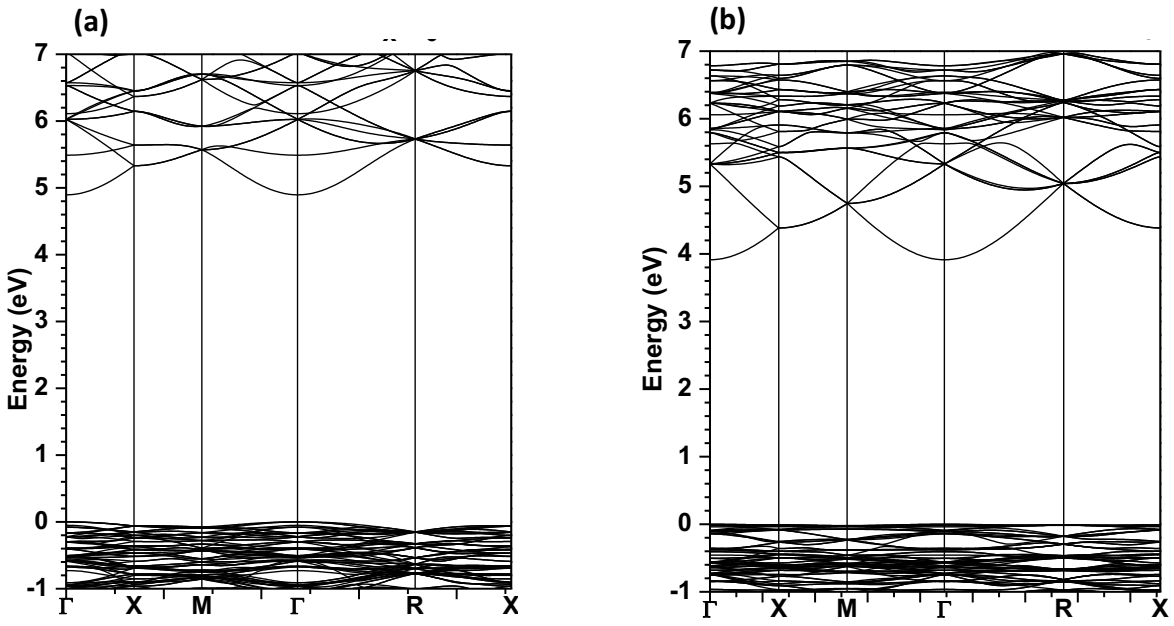

Figure 5 Calculated band structure for **(a)** grossular (x=0) and **(b)** katoite (x =3) . A full cubic cell is used instead of the primitive cell of bcc structure for the garnet.

function of x. Similar to other Si- or Al-based inorganic oxide crystals, the VB consists of two segments, the low segment (< -16 eV) with multiple peaks are from O-2s levels with different peak structures signaling a variety of local bonding environments of O to Si and Al. The upper segment (0.0 to -7 eV) comes from bonding orbitals of O-2p with Si and H orbitals and the non-bonding O-2p orbitals at the top of the VB. The HGS does not affect the band-gap significantly but their subtle variations in gap size and in spectral features in the VB and CB

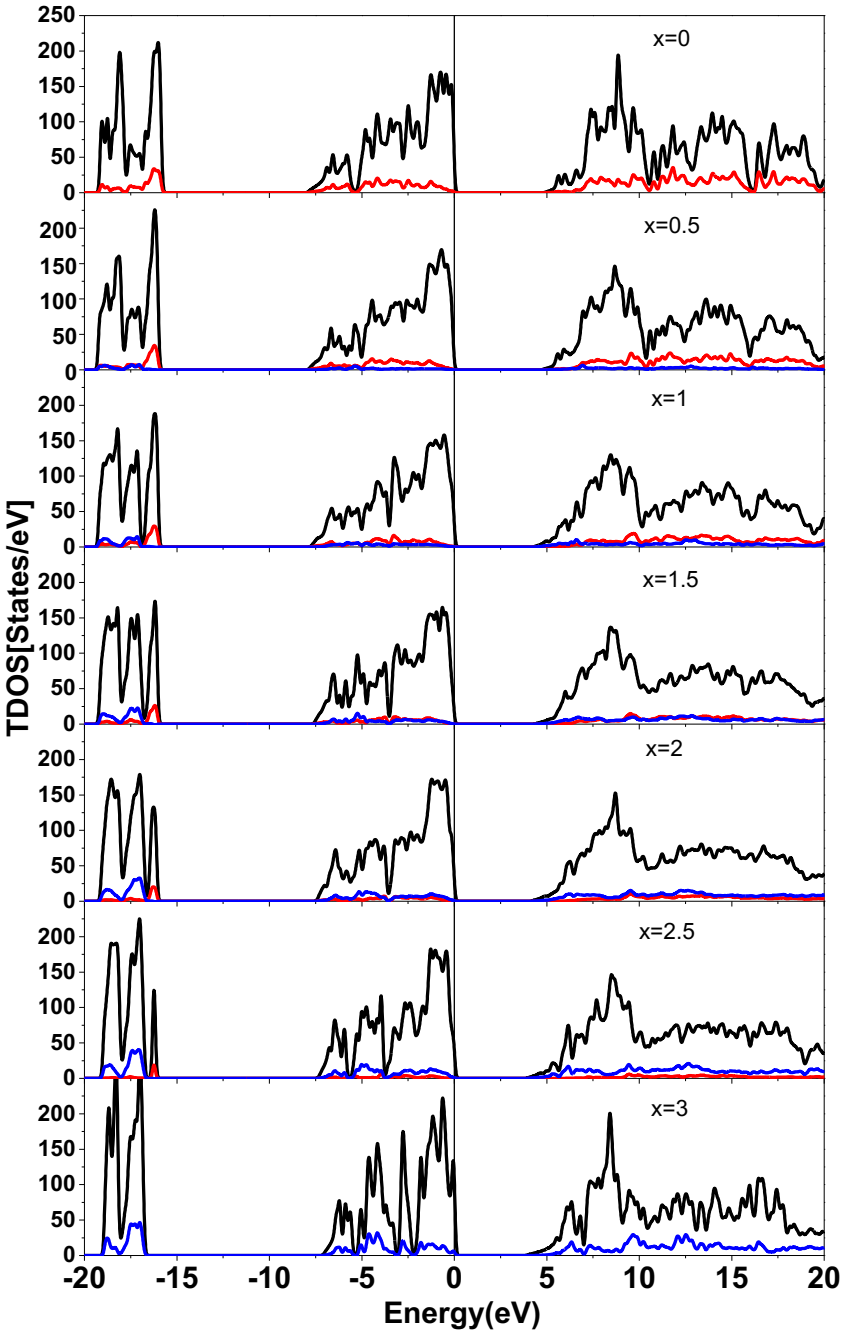

Figure 6 Calculated total density of states (TDOS) for hydrogrossular series $Ca_3Al_2(SiO_4)_{3-x}(OH)_{4x}$ (black line). The red and blue lines are partial density of states (PDOS) for silicon and hydrogen respectively.

could impact their optical properties (to be discussed in subsection 5.1.3). At x = 0 the VB peaks are broad but these peaks tend to separate and some become sharper at higher x. The VB of katoite shows clear separation of peaks. This indicates the change in bonding characters and the effect of hybridization as x is increased in the HG series. The CB show relatively minor changes with x = 0 and x = 3 display shaper peaks than the intermediate members of the HG series.

The ratio of H/Si atoms is a key factor in the HG series since it determines the intermediate members. For a more detailed analysis, we also show in **Fig. 6** the calculated PDOS of Si (red line) and H (blue line). As can be seen, both blue and red curves contribute equally at x = 1.5, the midpoint of 0 and 3 in HGS. In general, the contribution of Si and H to the PDOS is relative to the number of these atoms as x various. The band-gap reduces from 4.90 eV in x = 0 with no hydrogen to 3.91 eV at x = 3 with no Si. The values for the intermediate series at x = 0.5, 1, 1.5, 2, 2.5 are 4.75 eV, 4.32 eV, 4.37 eV, 4.20 eV and 3.94 eV respectively. This explains whole series are insulator.

5.1.2 Interatomic bonding

The bonding topology in the HG series may give additional insights to the effect of composition as x increases from the view point of internal crystal cohesion. The calculated bond order (BO) values is a measure of strength and stiffness of the bond for each atomic pairs [57]. Since HG can also be considered as a cement material, similar discussion on the BO in relation to crystal cohesion has been applied to the calcium silicate hydrates (CSH) crystals crystals [58]. There are five major types of bonding in HG series, roughly in the descending order of strength: covalent bonds (Si-O, O-H), ionic bond (Ca-O, Al-O) and Hydrogen bond (O···H). The calculated results are displayed in **Fig. 7(a)** for BO vs. bond length (BL) and in

Fig. 7(b) the corresponding number of the bond types and their average BO values (in unit of electrons) in 7 HG series.

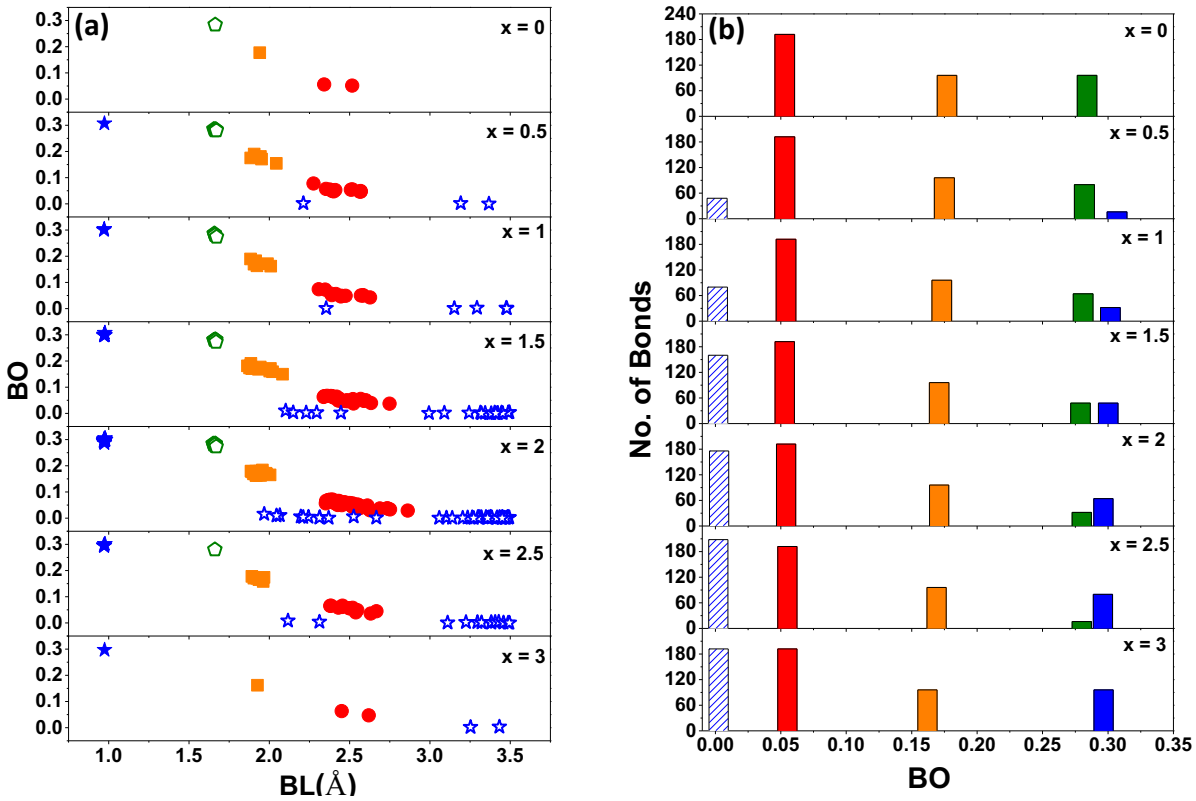

Figure 7 (a) Calculated bond order values vs. bond length as a function of x in hydrogrossular series. Ca-O (red solid circle), Al-O (orange solid square), Si-O (hollow green pentagon), O-H (solid blue), O···H (hollow blue star) is shown respectively. **(b)** Histogram distribution of number of each types of bonds as a function of x in hydrogrossular series. The Ca-O (red), Al-O (orange), Si-O (green), O-H (solid blue), O···H (striped blue) is shown respectively.

It should be noted that in HGS, the number for different types of bonds with different bond strengths varies as well as their optimized cell volume. [58]. In HG series, the strongest

bonds are the Si-O bonds having BO in the range 0.272-0.286 and BL from 1.651-1.681 Å. Both the BO values and BL for the Si-O bonds clustered within a very narrow range. This implies that SiO_4 tetrahedra are rigid and behave as a strong block. Thus interatomic bonding quantitatively justifies our criterion 1 descripted in Section 2. The presence of the O···H bonds when Si are replaced by H in the grossular substitution is a subject of great importance that has been speculated but not seriously discussed. It's clear from **Fig. 7** that the HB in HG series is non-existent or very weak because their BO values are close to zero and despite their increased abundance as x increases. This is in agreement with the experimental work on IR measurements by Geiger and Dachs in katoite [13]. Thus, HBs play no role in contributing to crystal cohesion in contrast to the CSH crystals [58]. It is also consistent with the fact that katoite has a much weaker mechanical properties than grossular (see section 5.2 below). The garnet substitution is often referred to as replacement of silicate tetrahedra with O_4H_4 tetrahedra,[8, 9, 59, 60] with implications of forming HBs. The BO values in **Fig.7** clearly show that the HBs are practically negligible and the assertion of hypothetical O_4H_4 tetrahedron could be fictitious. The situation could be completely different if real water molecules are present as oppose to the equally fictitious concept of "crystalline" water in describing the HG series. On the other hand, the covalent O-H bond is a very strong having BO values in the range 0.286-0.307 and a narrow BL range of 0.969- 0.981 Å. The hydroxyl O-H units, often considered as a separate unit, do not contribute to the connectivity between aluminate units. In fact, the covalent Al-O bonds are fairly strong with BO values ranging from 0.149- 0.191 and BL 1.864 - 2.082 Å. Their BO distribution is relatively wide indicating the flexibility of AlO_6 octahedra in forming a network with SiO_4 tetrahedra. The ionic Ca-O bonds are much weaker as observed in cement materials [58]. Their BO values are in the range of 0.029 - 0.077 with

much larger BL of 2.275-2.863 Å. They have a wide distribution for all members in the HG series. Thus Ca-O bonds play only a minor role in garnet substitution and in the stability of the structure since both the number of Ca ions and O ions remain the same. **Fig.7** vividly shows the change in the number of differ types of bonds, their distributions and different strengths resulting in a steady decrease in mechanical strength and crystal cohesion as x increases. Their specific variation depends on the crystal structure and associated interatomic bonding.

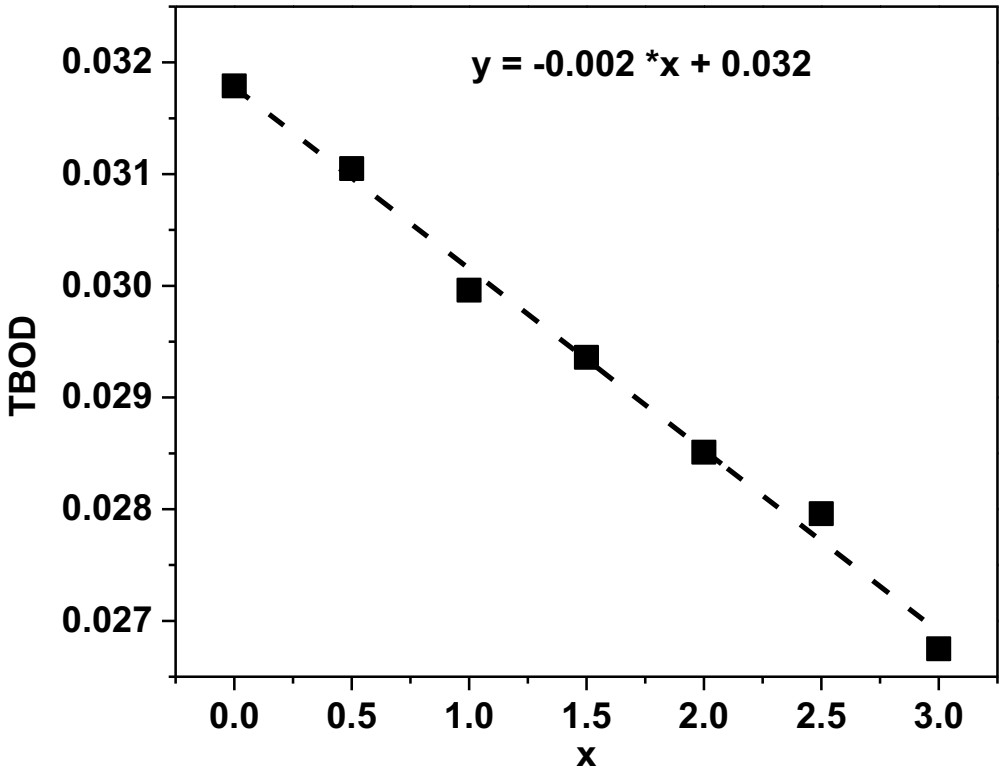

Figure 8 Variation of Total Bond order density (TBOD) shown as a function of composition (x). The dashed lines are linear fit.

A direct implication of the BO analysis in HG series is the important parameter total bond order density (TBOD). We have been advocating the use of TBOD as a single well-defined physical parameter which serves as a valid theoretical metric in assessing the overall cohesion of materials [53, 58]. Here, we apply the concept of TBOD to the HG series to gain additional insights. The variation of the calculated TBOD with x for HG series is shown in **Fig. 8**. There is a linear trend similar to other properties. The highest TBOD at x = 0 and the lowest is at x =3 as expected. The linear trend for the series is the result of subtle interplay of different types of bonds and structural variations and the way SiO_4 and AlO_6 units are distributed in the series. This is another example of using TBOD as a single quantum mechanical metric in describing the properties of complex multi-component materials.

5.1.3 Optical Properties

We have calculated the optical properties of the HG series in the form of complex dielectric function based on the interband optical transitions (See section 3). **Fig 9** shows the calculated real and imaginary parts of the frequency-dependent dielectric function (ε_1 and ε_2) for the HG series. The ε_2 is calculated first and ε_1 is obtained from ε_2 using Kramers Kronig conversion. For x = 0, there is ε_2 has two absorption peaks of 4.98 at 8.48 eV and 4.97 at 9.06. For x = 0.5, 1, 1.5, 2, 2.5 and 3 ε_2 has single absorption peak of 4.38 at 8.83 eV, 3.96 at 8.66 eV, 3.54 at 8.65 eV, 3.06 at 9.07 eV, 3.12 at 9.04 eV and 3.07 at 9.19 eV respectively. From the calculated dielectric functions, we can obtain the static dielectric constant by taking the zero frequency limit of the real parts of the dielectric function i.e., $\varepsilon_1(0)$. The refractive index can be approximated as the square root of $\varepsilon_1(0)$.

Optical absorption has been one of the properties that helps to identify the mineral groups [61]. In **Fig. 10**, we show the calculated refractive index n of HG series as a function

of x. Also shown is the experimental data from ref. [8]. Both show a linear trend of decreasing refractive index n as x increases. The calculated refractive index for HG series is higher than the experimental data. There are several possible explanations. One of them is that the calculations are based on the DFT which is strictly only valid for the ground state properties, less valid for optical transitions involving excited states.

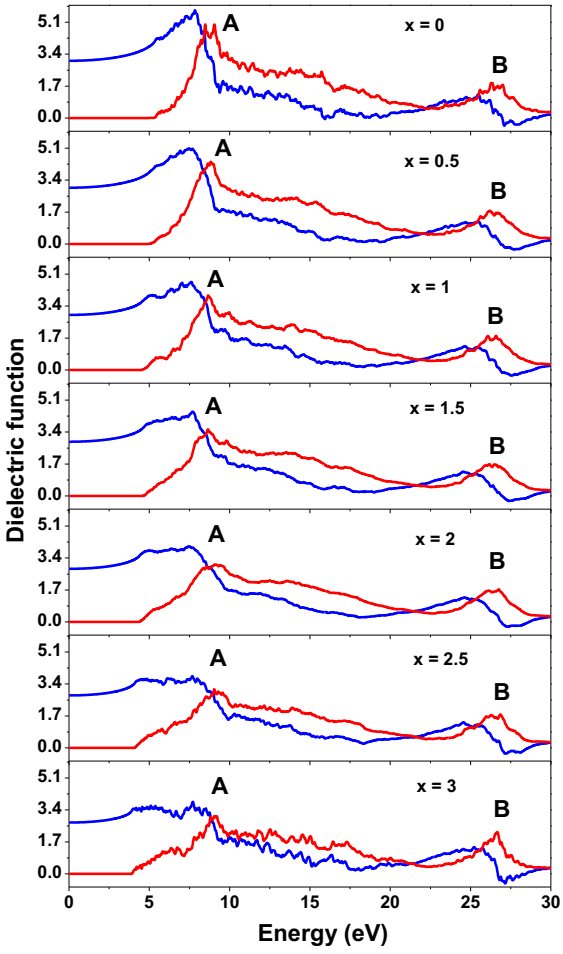

Figure 9 Calculated real (ε_1) (blue curve) and imaginary (ε_2) (red curve) parts of the dielectric function for HG series.

The calculation is basically at zero temperature whereas experimental measurement may be at room temperature on samples of unknown quality and definitely not on pure single crystals. Another reason for the differences in the experimental values may be due to the presence of impurity. For example, Foshag in 1924 [62, 63], showed that HG may contain CO_2 and H_2O with the chemical formula of [3CaO. Al_2O_3 2(SiO_2, CO_2) 2H_2O] [x = 1, n = 1.675]. Passalgia 1984 [5], worked on [$Ca_{2.96}(Al_{1.85}Mg_{0.01})(Si_{0.69}S_{0.11})O_{2.93}(OH)_{9.07}$] [x = 2, n = 1.632].

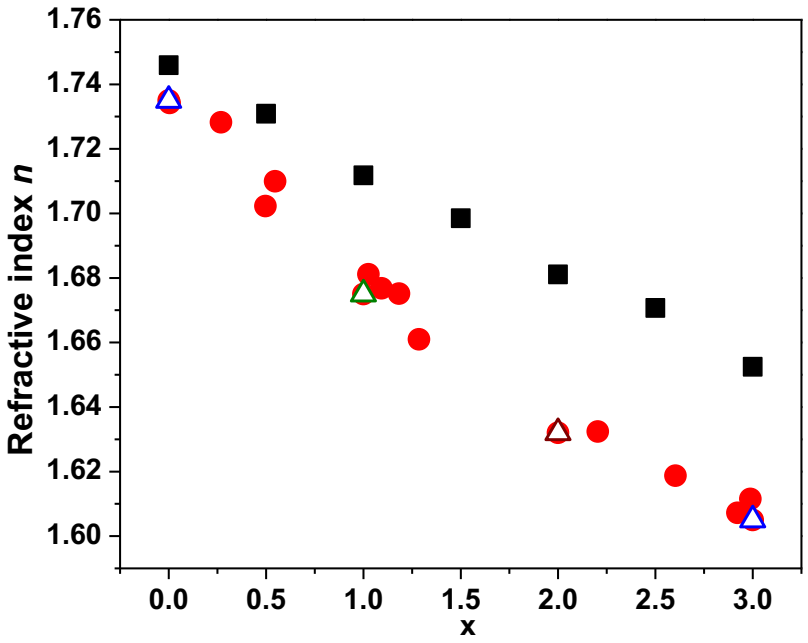

Figure 10 Calculated refractive index shown as a function of composition (x) shown in black square. The red circle shows the experimental values and hollow triangle [5, 8, 14, 63].

Furthermore, Flint in 1942 [14] synthesized the grossular and katoite and does not have any impurity but they mentioned that because of small size refractive index is not so accurate for grossular and plazolite (hibschite) [x = 3, n = 1.605] [x = 0, n =1.735].

5.2 Mechanical Properties of the Hydrogrossular series

5.2.1 Elastic Stiffness Constants and Bulk Mechanical Properties

The effect of the hydrogrossular substitution on the mechanical properties on HG series is an important piece of information for geologists to assess the composition and abundance of HG series crystals in the earth's crust with broader implication on geothermal process. The mechanical and elastic properties can be used to estimate the stability of the crystals in different hydro thermal conditions as well as in seismic studies. The elastic coefficients C_{ij} can provide data on elastic anisotropy. Cubic structures are elastically isotropic whereas tetragonal are not. The elastic constants for a cubic crystal are $C_{11} = C_{22} = C_{33}$, $C_{12} = C_{13} = C_{23}$ and $C_{44} = C_{55} = C_{66}$. For a tetragonal crystal, $C_{11} = C_{22}$, $C_{13} = C_{23}$; $C_{44} = C_{55}$ and the non-zero terms are C_{12}, C_{33} and C_{66}. The calculated elastic coefficients for each of the HG series using the method described in Chapter 3 are listed in **Table 3**. Experimentally, the reported elastic coefficients for grossular [$(Ca_{0.998}Mn_{0.002})_3(Al_{0.992}Fe_{0.008})_2Si_3O_{12}$] [7] are very close to our calculated values., The slight difference can be attributed to impurity content in the sample used in the experiment. The calculated elastic coefficients are used to obtain the mechanical parameters (bulk modulus (K), shear modulus (G), young's modulus (E)) for the series using VRH polycrystals approximation [64]. **Fig. 11 (a)** shows the calculated values of K, G, E as a function of x. They show an almost linear decrease of bulk mechanical properties

Table 3. Calculated elastic constants of HGS in GPa.

x	C_{11}	C_{12}	C_{44}	C_{13}	C_{33}	C_{66}	Remark
0	292.7	85.5	94.7				Cubic
0	*321.7*[a]	*91.4*[a]	*104.6*[a]				*Bass 1989*
0.5	237.7	57.0	81.9	70.3	228.4	73.5	Tetragonal
1	170.6	55.5	60.5	46.2	198.1	66.8	Tetragonal
1.5	148.3	44.1	55.18	43.62	174.5	57.0	Tetragonal
2	122.4	44.8	45.3	39.1	135.4	47.8	Tetragonal
2.5	112.4	34.8	40.9	37.3	111.4	36.4	Tetragonal
3	80.0	36.9	41.0				Cubic

a =[7]

Though there are some of the mechanical properties available for the end members experimentally they do not provide the information on how the changes goes on increasing the HGS in every individual intermediate stage. Therefore this calculation shows the effect of HGS and how the value changes does gradually. For a given crystal we observe the usual trend of E > K > G in all x in the series. Our results are in close agreement with some available experimental (open symbols in **Fig. 11(a)**) values [7, 9]. The experimental data on bulk modulus and shear modulus for x = 0 is from measurements by Bass [7] on a sample with nominal composition of $[Ca_{0.998}Mn_{0.002})_3(Al_{0.992}Fe_{0.008})_2Si_3O_{12}]$. The presence of minor traces

of impurities may be the reason of for a very small difference. It is well known fact that katoite is far more compressible than grossular since O_4H_4 is highly compressible [10].

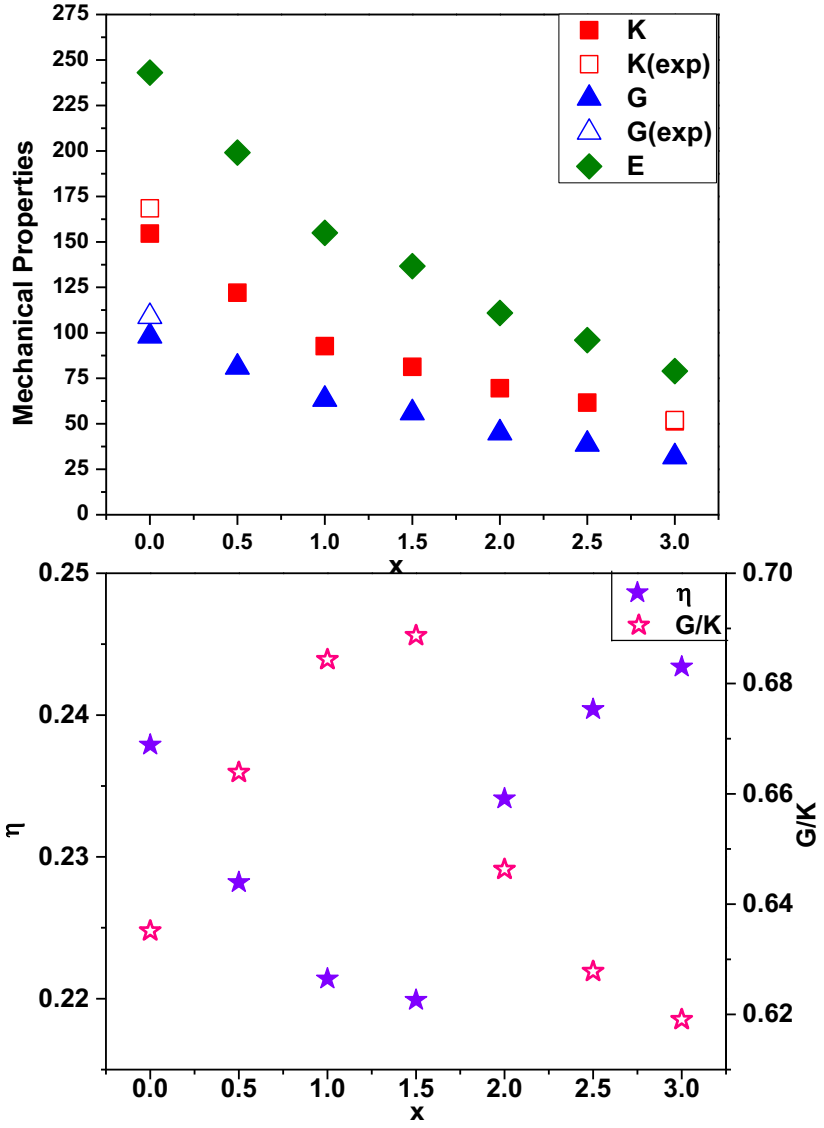

Figure 11(a) Calculated mechanical properties of bulk modulus(K)**,** shear modulus(G), youngs modulus(E) as a function of composition x**.** The experimental data [7, 9] are represented in open symbols. **(b)** poisson ratio (η) and pugh moduli ratio(G/K) as a function of compostion (x).

As we have argued in the earlier section that when Si is replaced by 4H in the HGS, it gradually weakens the structure as the x increased.

Fig. 11(b) shows the plot of the Poisson's ratio η and the Pugh moduli ratio G/K for the HG series. They can be considered as more balanced overall parameters in assessing the mechanical properties of a crystal in relation to brittleness or ductility of a material [65].

η and G/K are almost inverse to each other except in the very extreme cases. A low G/K or a higher η indicates the materials is more ductile or less brittle. Our calculations indicate that grossular is strong and brittle where as katoite can be quite ductile. The intermediate members shows variation. Poisson ratio and pugh moduli ratio looks more irregular than other bulk properties. This is because the poisson ratio depends on the ratio of K and G. In **fig.11(a)** we can see that the slope of K and G changes from x = 1.5, they change in such a way showing slightly different graph pattern for the poisson ratio and pugh moduli ratio. The poisson ratio decreases till x = 1.5 and then increases to x =3. Inversely pugh moduli ratio increases till x = 1.5 and then decreases to x = 3.

6. CONCLUSION

In this thesis we have presented a method and obtained the stable structures for the intermediate members of the hydrogrossular mineral series $Ca_3Al_2(SiO_4)_{3-x}(OH)_{4x}$. An in-depth analysis in term of the structure, electronic, mechanical and optical properties all support the existence of a competition from cubic to tetragonal phase for $x > 0$ and less than 3. This is the result of symmetry lowering transition when Si atoms are progressively replaced by H atoms in 1: 4 ratio that has not been revealed previously and can be related to the symmetry in the composition of SiO_4 tetrahedra and AlO_6 octahedra in the process of hydrogarnet substitution. The calculated physical properties such as the lattice constant, mechanical properties, refractive index etc., especially for the end members grossular (x=0) and Katoite (x=3) agree well with the existing experimental data thus giving credence to our results for the whole HG series. Mechanical properties will be very helpful to obtain the seismic wave velocities and also characterize the mineral series. It can be used as data base for the geophysics deep analysis regarding earth mantle and its changes. Refractive index obtained from the optical properties of the complete series can be used to characterize the minerals series. Though not very close to the experimental result however, it can be used as an estimation.

Of particular importance is the use of total bond order density (TBOD) a single quantum mechanical metric to assess the strength and internal cohesion for the HG series based on the extensive data of various types of chemical bonds present in the mineral series and their changes a function of x. TBOD provides information of the mineral series getting weaker as there is increase in hydrogarnet substitution.

We specifically point out the inappropriateness of using the ill-defined concept of treating O_4H_4 as a compressible structural unit in interpreting the structure and properties of

HG series. Since O-H bond is the slightly stronger and acts as single bond unit instead of support to the whole system like Si-O bond (forming SiO_4 tetrahedral), therefore is one of the cause for the more compressibility as the value of x increases from grossular. The so-called hydrogen bonds in the series are very weak and should not be confused with the traditional HB with the presence of real water molecules (H_2O) whose presence can significantly change many of the physical properties. In other words, the present study reveal the drawbacks of the traditional concepts prevailing in the geophysical community regarding the hydration process of the grossular minerals or other similar minerals which has profound implications in the interpretation geochemical data on Earth's mantle and their compositions. The potential presence of water molecules in Earth mineral including the hydrogrossular series cannot be denied and will result in very different properties. Finally, the present work demonstrates the important role played by large-scale computations in solving problems where experimental techniques are impossible or difficult to apply.

6.1 Future Work

We intend to extend this work with phonon calculations. Structure and physical properties of clay minerals has always been a matter of great interest especially in multidisciplinary area of physics, chemistry, materials science geology and earth science. In particular, the atomic composition, electronic structure, interatomic bonding, charge transfer, optical properties and mechanical properties that can help elucidate the fundamental issues such as bond strength, solvation effect, spectral characterization, optical absorption, elasticity, seismic wave velocities etc. are most valuable. Although there have been considerable experimental studies on clay minerals, detailed information on their structure and properties are still lacking. Ab initio computational research appears to be the most suitable to obtain

such information due to recent development in supercomputing technology in contrast to the costly experimental trial-and-error approach in laboratory. We intend to use similar approach to study other equally important and more complex clay or mineral materials such as montmorillonite, Kaolinite, muscovite etc, for which the electronic structure and bonding information are totally unknown. They have far more complicated structures and compositions and under different thermodynamic conditions of pressure and temperature.

APPENDIX

INCAR file

System = Si24Al16Ca24O96

ISMEAR = 0 ! Use 0 for KPOINTS less than 4 otherwise -5.

PREC = Accurate ! low, medium, normal are other options. Use suitable one.

ENCUT = 600 eV ! Decide considering the crystal size and accuracy you want.

EDIFF = $1.0E^{-5}$! Energy difference convergence limit for electronic optimization.

EDIFFG = $-1.0E^{-3}$! Energy difference convergence limit for ionic optimization.

IBRION = 1 ! 0 for MD, 1 best, 2 for diff relaxation problems.

NSW = 800 ! Total number of ionic steps.

ISIF = 3 ! 2 and 4 ionic, 7 volume and 3 both.

LREAL = Auto ! Projection on real space. Use FALSE (default) for reciprocal space.

NPAR = 7 ! Square root of NCPU used

ALGO = Fast ! Default is Normal.

LCHARG = F ! No writing in CHG and CHGCAR files

LWAVE = F ! No writing in WAVECAR file

KPOINT file

Automatic generation

G

0 ! 0 means automatic generation scheme

G ! G means gamma centered grid

1 1 1 ! Subdivisions along the reciprocal lattice vectors

0 0 0 ! Optional shift of the mesh

BIBLIOGRAPHY

1. McConnell, D., *Griphite, a hydrophosphate garnetoid.* American Mineralogist, 1942. **27**(6): p. 452-461.
2. Pertlik, F., *Bibliography of hibschite, a hydrogarnet of grossular type.* GeoLines, 2003. **15**: p. 113-119.
3. Aines, R.D. and G.R. Rossman, *Water in minerals? A peak in the infrared.* Journal of Geophysical Research: Solid Earth (1978–2012), 1984. **89**(B6): p. 4059-4071.
4. Bell, D.R. and G.R. Rossman, *Water in Earth's mantle: the role of nominally anhydrous minerals.* Science, 1992. **255**(5050): p. 1391-1397.
5. Passaglia, E. and R. Rinaldi, *Katoite, a new member of the Ca3Al2 (SiO4) 3-Ca3Al2 (OH) 12 series and a new nomenclature for the hydrogrossular group of minerals.* Bull. Mineral, 1984. **107**: p. 605-618.
6. Cohen-Addad, C., et al., *Détermination de la position des atomes d'hydrogène dans l'hydrogrinat Al2O3, 3CaO, 6H2O par résonance magnétique nucléaire et diffraction neutronique.* Journal de Physique, 1964. **25**(5): p. 478-483.
7. Bass, J.D., *Elasticity of grossular and spessartite garnets by Brillouin spectroscopy.* Journal of Geophysical Research: Solid Earth (1978–2012), 1989. **94**(B6): p. 7621-7628.
8. O'Neill, B., J.D. Bass, and G.R. Rossman, *Elastic properties of hydrogrossular garnet and implications for water in the upper mantle.* Journal of Geophysical Research: Solid Earth (1978–2012), 1993. **98**(B11): p. 20031-20037.
9. Lager, G.A. and R.B. Von Dreele, *Neutron powder diffraction study of hydrogarnet to 9.0 GPa.* American Mineralogist, 1996. **81**(9-10): p. 1097-1104.
10. Knittle, E., et al., *A spectroscopic Study of the High-Pressure Behavior of the O4H4 Substitution in Garnet*, in *High-Pressure Research: Application to Earth and Planetary Sciences*. 2013, American Geophysical Union. p. 297-304.
11. Martin, R.F. and G. Donnay, *Hydroxyl In Mantle.* American Mineralogist, 1972. **57**(3-4): p. 554-570.
12. Geiger, C.A., E. Dachs, and A. Benisek, *Thermodynamic behavior and properties of katoite (hydrogrossular): A calorimetric study.* American Mineralogist, 2012. **97**(7): p. 1252-1255.
13. Geiger, C. and E. Dachs. *An IR and calorimetric investigation of the structural, crystal-chemical and thermodynamic properties of hydrogrossular*. in *EGU General Assembly Conference Abstracts*. 2012.
14. Flint, E.P., H. McMurdie, and L.S. Wells, *Hydrothermal and X-ray studies of the garnet-hydrogarnet series and the relationship of the series to hydration products of portland cement.* Journal of Research of the National Bureau of Standards, 1941. **26**(1): p. 13-33.
15. Lager, G., T. Armbruster, and J. Faber, *Neutron and X-ray diffraction study of hydrogarnet Ca 3 Al 2 (O 4 H 4) 3.* American Mineralogist, 1987. **72**(7-8): p. 756-765.
16. Schoenitz, M. and A. Navrotsky, *Enthalpy of formation of katoite Ca3Al2 [(OH) 4] 3: Energetics of the hydrogarnet substitution.* American Mineralogist, 1999. **84**: p. 389-391.

17. Erba, A., et al., *Katoite under pressure: an ab initio investigation of its structural, elastic and vibrational properties sheds light on the phase transition.* Physical Chemistry Chemical Physics, 2015. **17**(4): p. 2660-2669.
18. Anrvrnnusrnn, T., J. Fn-q Nr, and G.R. RossvHN, *OH substitution in garnets: X-ray and neutron diffraction, infrared, and geometric-modeling studies.* American Mineralogist, 1989. **74**: p. 840-851.
19. Nobes, R., et al., *Structure and properties of aluminosilicate garnets and katoite: an ab initio study.* Computational Materials Science, 2000. **17**(2): p. 141-145.
20. Orlando, R., et al., *Vibrational spectrum of katoite Ca3Al2 [(OH) 4] 3: a periodic ab initio study.* The Journal of Physical Chemistry B, 2006. **110**(2): p. 692-701.
21. Zicovich-Wilson, C.M., et al., *Ab initio simulation of the IR spectra of pyrope, grossular, and andradite.* Journal of computational chemistry, 2008. **29**(13): p. 2268-2278.
22. Erba, A., et al., *Elastic properties of six silicate garnet end members from accurate ab initio simulations.* Physics and Chemistry of Minerals, 2014. **41**(2): p. 151-160.
23. Lacivita, V., et al., *Elasticity of grossular–andradite solid solution: an ab initio investigation.* Physical Chemistry Chemical Physics, 2014. **16**(29): p. 15331-15338.
24. Parr, R.G. and W. Yang, *Density-functional theory of atoms and molecules*. Vol. 16. 1989: Oxford university press.
25. Hohenberg, P. and W. Kohn, *Inhomogeneous electron gas.* Physical review, 1964. **136**(3B): p. B864.
26. Kresse, G. and J. Hafner, *Ab initio molecular dynamics for liquid metals.* Physical Review B, 1993. **47**(1): p. 558.
27. Kresse, G. and J. Furthmüller, *Software VASP, vienna (1999).* Phys. Rev. B, 1996. **54**(11): p. 169.
28. Vanderbilt, D., *Soft self-consistent pseudopotentials in a generalized eigenvalue formalism.* Physical Review B, 1990. **41**(11): p. 7892.
29. Kresse, G. and J. Hafner, *Norm-conserving and ultrasoft pseudopotentials for first-row and transition elements.* Journal of Physics: Condensed Matter, 1994. **6**(40): p. 8245.
30. Blöchl, P.E., *Projector augmented-wave method.* Physical Review B, 1994. **50**(24): p. 17953.
31. Kresse, G. and D. Joubert, *From ultrasoft pseudopotentials to the projector augmented-wave method.* Physical Review B, 1999. **59**(3): p. 1758.
32. Perdew, J.P., K. Burke, and M. Ernzerhof, *Generalized gradient approximation made simple.* Physical review letters, 1996. **77**(18): p. 3865.
33. Ching, W., *Theoretical studies of the electronic properties of ceramic materials.* Journal of the American Ceramic Society, 1990. **73**(11): p. 3135-3160.
34. Ching, W.-Y. and P. Rulis, *Electronic Structure Methods for Complex Materials: The orthogonalized linear combination of atomic orbitals*. 2012: Oxford University Press.
35. Liang, L., P. Rulis, and W. Ching, *Mechanical properties, electronic structure and bonding of α-and β-tricalcium phosphates with surface characterization.* Acta biomaterialia, 2010. **6**(9): p. 3763-3771.
36. Ching, W., et al., *Electronic structure and physical properties of the spinel-type phase of BeP 2 N 4 from all-electron density functional calculations.* Physical review B, 2011. **83**(15): p. 155109.

37. Ching, W., et al., *Theoretical study of the elasticity, mechanical behavior, electronic structure, interatomic bonding, and dielectric function of an intergranular glassy film model in prismatic β-Si 3 N 4.* Physical Review B, 2010. **81**(21): p. 214120.
38. Rulis, P. and W. Ching, *Theoretical ELNES spectra of Si-K, Si-L, NK, and OK edges of an intergranular glassy film model in β-Si3N4.* Journal of materials science, 2011. **46**(12): p. 4191-4198.
39. Adhikari, P., et al., *Electronic Structure, Dielectric Response, and Surface Charge Distribution of RGD (1FUV) Peptide.* Scientific reports, 2014. **4**.
40. Eifler, J., et al., *Computational Study of a Heterostructural Model of Type I Collagen and Implementation of an Amino Acid Potential Method Applicable to Large Proteins.* Polymers, 2014. **6**(2): p. 491-514.
41. Poudel, L., et al., *Electronic structure, stacking energy, partial charge, and hydrogen bonding in four periodic B-DNA models.* Physical Review E, 2014. **90**(2): p. 022705.
42. Herring, C., *A new method for calculating wave functions in crystals.* Physical Review, 1940. **57**(12): p. 1169.
43. Mulliken, R., *Electronic population analysis on LCAO–MO molecular wave functions. II. Overlap populations, bond orders, and covalent bond energies.* The Journal of Chemical Physics, 1955. **23**(10): p. 1841-1846.
44. Mulliken, R.S., *Electronic population analysis on LCAO–MO molecular wave functions. I.* The Journal of Chemical Physics, 1955. **23**(10): p. 1833-1840.
45. Greenwood, D., *The Boltzmann equation in the theory of electrical conduction in metals.* Proceedings of the Physical Society, 1958. **71**(4): p. 585.
46. Winkler, B., *An introduction to" Computational Crystallography".* Zeitschrift fur Kristallographie, 1999. **214**: p. 506-527.
47. Stadler, R., et al., *Ab initio calculations of the cohesive, elastic, and dynamical properties of CoSi 2 by pseudopotential and all-electron techniques.* Physical Review B, 1996. **54**(3): p. 1729.
48. Nielsen, O. and R.M. Martin, *First-principles calculation of stress.* Physical Review Letters, 1983. **50**(9): p. 697.
49. Voigt, W., *Lehrbuch der kristallphysik (mit ausschluss der kristalloptik)*. 1928, Leipzig; Berlin: B.G. Teubner.
50. Reuss, A., *Berechnung der Fließgrenze von Mischkristallen auf Grund der Plastizitätsbedingung für Einkristalle.* ZAMM-Journal of Applied Mathematics and Mechanics/Zeitschrift für Angewandte Mathematik und Mechanik, 1929. **9**(1): p. 49-58.
51. Hill, R., *The elastic behaviour of a crystalline aggregate.* Proceedings of the Physical Society. Section A, 1952. **65**(5): p. 349.
52. GIBBS, G.N.A.G., *The crystal chemistry of the silicate garnets.* The American Mineralogist, 1971. **56**.
53. Dharmawardhana, C.C., et al., *Role of interatomic bonding in the mechanical anisotropy and interlayer cohesion of CSH crystals.* Cement and Concrete Research, 2013. **52**(0): p. 123-130.
54. Basso, R., A. Dellagiusta, and L. Zefiro, *CRYSTAL-STRUCTURE REFINEMENT OF PLAZOLITE-A HIGHLY HYDRATED NATURAL HYDROGROSSULAR.* Neues Jahrbuch Fur Mineralogie-Monatshefte, 1983(6): p. 251-258.

55. Xu, Y.-N. and W. Ching, *Electronic structure of yttrium aluminum garnet (Y 3 Al 5 O 12).* Physical Review B, 1999. **59**(16): p. 10530.
56. Ching, W. and Y.-N. Xu, *Nonscalability and nontransferability in the electronic properties of the Y-Al-O system.* Physical Review B, 1999. **59**(20): p. 12815.
57. Haslingerova, I., *Estimation of bond energies from mulliken overlap populations.* Czechoslovak Journal of Physics B, 1977. **27**(12): p. 1389-1393.
58. Dharmawardhana, C.C., A. Misra, and W.-Y. Ching, *Quantum Mechanical Metric for Internal Cohesion in Cement Crystals.* Sci. Rep., 2014. **4**.
59. Ferro, O., et al., *A new occurrence of katoite and re-examination of the hydrogrossular group.* European Journal of Mineralogy, 2003. **15**(2): p. 419-426.
60. Antao, S.M., *Crystal chemistry of birefringent hydrogrossular.* Physics and Chemistry of Minerals, 2015. **42**(6): p. 455-474.
61. Hutton, C.O. *Hydrogrossular, a new mineral of the garnet-hydrogarnet series*. in *Royal Society of New Zealand Transactions and Proceedings*. 1943.
62. Foshag, W., *Plazolite, a new mineral.* American Mineralogist, 1920. **5**: p. 183-185.
63. Foshag, W., *Plazolite, a new mineral corrections.* The American Mineralogist, 1924. **5**: p. 184.
64. Yao, H., L. Ouyang, and W.Y. Ching, *Ab initio calculation of elastic constants of ceramic crystals.* Journal of the American Ceramic Society, 2007. **90**(10): p. 3194-3204.
65. Pough, S., *Relations between the elastic moduli and the plastic properties of polycrystalline pure metals [J]*. Philosophical Magazine, 1954. **45**: p. 823-843.

VITA

Puja Adhikari was born on 1988 in Biratnagar Nepal. She finished her schooling from Bagmati Awasiya Ma Vi in 2003. Then finished her high school from NIC H S School, in 2005. In 2008 she completed her bachelor's degree from National Multiple College of Tribhuvan University. She got her master's degree from Golden Gate International College of Tribhuvan University in 2010.

She arrived to University of Missouri-Kansas City as a graduate student on July 2013. She was working as a graduate research assistant (GRA) in Electronic Structure Group (ESG) under supervison of Professor Dr. Wai-Yim Ching during her master's. She plans to continue her studies and research in UMKC.

Ms. Adhikari's one of research has been published in *Scientific Reports*. She has presented one talk in American Ceramic Society Cements Division meeting 6th Advances in Cement-based Materials (2015).